



MSU Graduate Theses


Spring 2017

FTIR Spectroscopy of Hot Exoplanets: A First Step in Experimental Procedure and Analysis

Heath Emmanuel Gemar

As with any intellectual project, the content and views expressed in this thesis may be considered objectionable by some readers. However, this student-scholar's work has been judged to have academic value by the student's thesis committee members trained in the discipline. The content and views expressed in this thesis are those of the student-scholar and are not endorsed by Missouri State University, its Graduate College, or its employees.

Follow this and additional works at: <https://bearworks.missouristate.edu/theses>

 Part of the [Materials Science and Engineering Commons](#)

Recommended Citation

Gemar, Heath Emmanuel, "FTIR Spectroscopy of Hot Exoplanets: A First Step in Experimental Procedure and Analysis" (2017). *MSU Graduate Theses*. 3165.
<https://bearworks.missouristate.edu/theses/3165>

This article or document was made available through BearWorks, the institutional repository of Missouri State University. The work contained in it may be protected by copyright and require permission of the copyright holder for reuse or redistribution.

For more information, please contact BearWorks@library.missouristate.edu.

**FTIR SPECTROSCOPY OF HOT EXOPLANETS: A FIRST STEP IN
EXPERIMENTAL PROCEDURE AND ANALYSIS**

A Master's Thesis

Presented to

The Graduate College of

Missouri State University

In Partial Fulfillment

Of the Requirements for the Degree

Master of Science, Materials Science

By

Heath Gemar

May, 2017

Copyright 2017 by Heath Emmanuel Gemar

FTIR SPECTROSCOPY OF HOT EXOPLANETS: A FIRST STEP IN EXPERIMENTAL PROCEDURE AND ANALYSIS

Physics, Astronomy, and Materials Science

Missouri State University, May 2017

Master of Science

Heath Gemar

ABSTRACT

In this thesis, I demonstrate how I constructed a complete experimental package to view FTIR Spectroscopy of constituents that make up hot, rocky exoplanets. I examine in detail the engineering and construction of such a system. Also, I developed a full computational package to analyze spectra in association and relate the analysis to that of real world application. The new system produces reproducible IR spectra on exoplanet analogs and can be used to probe complex chemistry composition at high temperatures.

KEYWORDS: FTIR spectroscopy, hot exoplanets, matlab analysis, spectral data, high temperature engineering.

This abstract is approved as to form and content

Dr. David Cornelison
Chairperson, Advisory Committee
Missouri State University

**FTIR SPECTROSCOPY OF HOT EXOPLANETS: A FIRST STEP IN
EXPERIMENTAL PROCEDURE AND ANALYSIS**

By

Heath Gemar

A Master's Thesis
Submitted to the Graduate College
Of Missouri State University
In Partial Fulfillment of the Requirements
For the Degree of Master of Science, Materials Science

May 2017

Approved:

Dr. David Cornelison

Dr. Mike Reed

Dr. Robert Mayanovic

Dr. Julie Masterson: Dean, Graduate College

ACKNOWLEDGEMENTS

I would like to thank the following people for their support during the course of my graduate studies:

Dr. David Cornelison

Dr. Mike Reed

Dr. Kartik Ghosh

Dr. Bob Mayanovic

Denny Bosch

Michal Bulak

Nolan Ingersol

Trey Grimes

Dr. Nathan Jacobson

Brian Grindstaff

Jonathan Keeth

TABLE OF CONTENTS

Introduction.....	1
Extra Solar Planets.....	1
Atmospheres	4
Lab Work	8
Theory.....	10
Fourier Transform Infrared Spectroscopy	10
Knudsen Cells	12
Matrix Isolation.....	14
Engineering	16
Chamber Design.....	16
E-Beam Evaporator.....	17
IR Optical Path.....	19
Thickness Monitor	22
Gas Inlet.....	23
Thermometry.....	25
Experimental	26
Programming Results.....	28
LabVIEW	28
Omnice.....	29
Matlab	29
Engineering Results	31
Gas Inlet.....	31
Emissivity	31
Scientific Results	35
SiO	35
Si ₂ O ₂	39
Si ₃ O ₃	42
Discussion	46
References.....	47
Appendices	49
Appendix A: Analyzing Spectra Code.....	49
Appendix B: Emissivity Correction Code	60

LIST OF FIGURES

Figure 1. Credit N. Batalha, PNAS 2014.....	1
Figure 2. Artist's Depiction of Kepler 10b (NASA/Kepler Mission/Dana Berry).....	2
Figure 3. Showing HD 209458 off axis in comparison with Jupiter. (NASA, ESA, and A. Feild [STScI]).....	3
Figure 4. Atmospheric gas composition for CoRoT-7b assuming 2500 K temperature and 10-2 bar pressure for two alternate compositions, calculated using MAGMA (Schaefer et al 2012).	5
Figure 5. Showing the variation of brightness from both star and planet while in orbit of 55 Cancri e. (NASA/JPL - Caltech/University of Cambridge).....	6
Figure 6. Spectrum of sunlight (black) and sunlight that has passed through Earth's atmosphere (red) (ASTM 2012).....	7
Figure 7. A Michelson Interferometer. (http://pe2bz.philpem.me.uk/)	11
Figure 8. Graphical depiction of a Fourier Transform from frequency space to time space. (UC, Davis/ Jing Zhao).....	12
Figure 9. Depiction of Knudsen Cell	13
Figure 10. Spherical chamber in process of building set up. (Heath Gemar).....	16
Figure 11. Spherical CAD design. (John Lester).....	17
Figure 12. E-Beam Evaporator post-run. Flakes are cooled SiO fallen from cooling shroud. (Heath Gemar).....	18
Figure 13. Cooling shroud and shutter set up from underneath the chamber. (Heath Gemar)	19
Figure 14. Optical pathway going into the chamber from the IR source. (Heath Gemar) 20	
Figure 15. Copper mirror used as flag within the system. (Michal Bulak)	21
Figure 16. Optical pathway exiting the chamber. (Heath Gemar).....	21
Figure 17. Graphical representation of Au, Al, and Ag as a function of wavelength. Showing Au to be the best choice for mirrors given our wavelength. (Bob Mellish)	22
Figure 18. Optical pathway of the thickness monitor. Depiction of where the path difference occurs. (Heath Gemar).....	23

Figure 19. Depiction of the two separate gas inlet designs. The left having a series of holes while the right has a series of tubes leading to the center. (Heath Gemar)	24
Figure 20. Picture of actual prong gas inlet. (Michal Bulak).....	24
Figure 21. Interference pattern showing the growth rate of Ar ice using the Ring system at 3×10^{-6} Torr.	32
Figure 22. Interference pattern showing the growth rate of Ar Ice using the prong system at 3×10^{-7} , 6.7×10^{-7} , and 3×10^{-6} Torr.	32
Figure 23. Graph showing the curve fitted to NIST data on Ta emissivity change with temperature.	33
Figure 24. Graph showing the relationship between the measure temperature and true temperature as explained through the text.	34
Figure 25. Use of the Matlab code developed to analyze the IR spectra observed. SiO peak 10 minutes after the shutter was opened at 1600 C.	36
Figure 26. Use of the Matlab code developed to analyze the IR spectra observed. SiO peak 20 minutes after the shutter was opened at 1600 C.	36
Figure 27. Use of the Matlab code developed to analyze the IR spectra observed. SiO peak 30 minutes after the shutter was opened at 1600 C.	37
Figure 28. Use of the Matlab code developed to analyze the IR spectra observed. SiO peak 40 minutes after the shutter was opened at 1600 C.	37
Figure 29. Use of the Matlab code developed to analyze the IR spectra observed. SiO peak 50 minutes after the shutter was opened at 1600 C.	38
Figure 30. Graphical depiction of the Area Progression of the main SiO peak. Shutter was open and depositing for 50 minutes at 1600 C.	38
Figure 31. Use of the Matlab code developed to analyze the IR spectra observed. Si ₂ O ₂ peak 10 minutes after the shutter was opened at 1600 C. There was no evidence after this amount of time that any Si ₂ O ₂ was deposited.	39
Figure 32. Use of the Matlab code developed to analyze the IR spectra observed. Si ₂ O ₂ peak 20 minutes after the shutter was opened at 1600 C.	40
Figure 33. Use of the Matlab code developed to analyze the IR spectra observed. Si ₂ O ₂ peak 30 minutes after the shutter was opened at 1600 C.	40
Figure 34. Use of the Matlab code developed to analyze the IR spectra observed. Si ₂ O ₂ peak 40 minutes after the shutter was opened at 1600 C.	41

Figure 35. Use of the Matlab code developed to analyze the IR spectra observed. Si_2O_2 peak 50 minutes after the shutter was opened at 1600 C.....	41
Figure 36. Graphical representation of the area progression of the main Si_2O_2 peak for 50 minutes at 1600C.	42
Figure 37. Use of the Matlab code developed to analyze the IR spectra observed. Si_3O_3 peak 10 minutes after the shutter was opened at 1600 C. There was no evidence after this amount of time that any Si_3O_3 was deposited.	43
Figure 38. Use of the Matlab code developed to analyze the IR spectra observed. Si_3O_3 peak 20 minutes after the shutter was opened at 1600 C.....	43
Figure 39. Use of the Matlab code developed to analyze the IR spectra observed. Si_3O_3 peak 30 minutes after the shutter was opened at 1600 C.....	44
Figure 40. Use of the Matlab code developed to analyze the IR spectra observed. Si_3O_3 peak 40 minutes after the shutter was opened at 1600 C.....	44
Figure 41. Use of the Matlab code developed to analyze the IR spectra observed. Si_3O_3 peak 50 minutes after the shutter was opened at 1600 C.....	45
Figure 42. Graphical representation of the area progression of the main Si_3O_3 peak for 50 minutes at 1600C.	45

INTRODUCTION

Extra Solar Planets

The Kepler spacecraft launched in 2009, and since then, has revolutionized the extrasolar planetary research. However, research into exoplanets in general has been booming since the 1990's, with thousands found up to the current time. These exoplanets exhibit a wide range of orbit dimensions, and can be massive Jupiter-like, or smaller more earth-sized bodies (Armitage 2010, Elkins-Tanto and Seager 2008, Winn, Matthews, and Dawson 2011). In this thesis, we will consider parameters associated with short-period, rocky exoplanets and their atmospheric impact to their blackbody curve. Below is Figure 1 depicting the number of exoplanets observed with relation to planets from our own solar system.

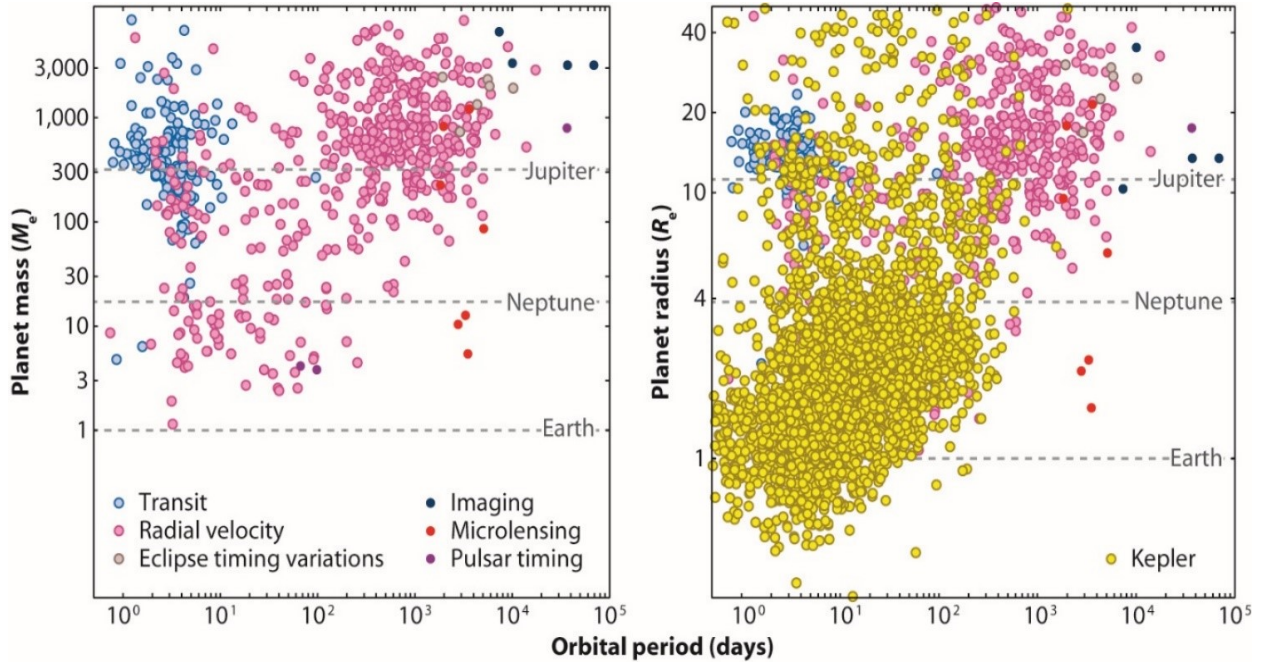


Figure 1. Credit N. Batalha, PNAS 2014.

Rocky planets in orbits close to their star are likely to have high surface temperatures, in some cases greater than 2000 K. Such planets would have an atmosphere of rock vapor, different from any planets within our own solar system.

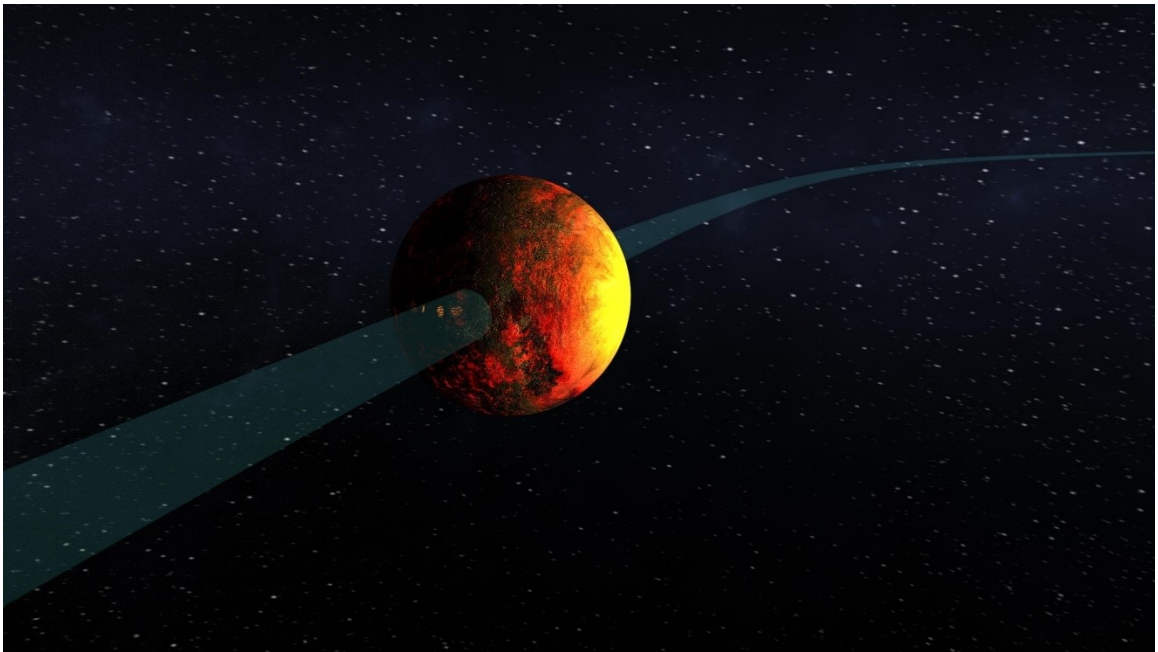


Figure 2. Artist's Depiction of Kepler 10b (NASA/Kepler Mission/Dana Berry)

Kepler 10b was the first planet discovered by the Kepler mission with such properties. The planet is 4.6 times more massive than the Earth, while having a radius 1.5 times more than that of the Earth, and orbiting at a distance $1/60^{\text{th}}$ of that of Earth to the Sun. These factors lead to day-side temperatures of 3316 K and night side temperatures of 2600 K. At these extreme temperatures, the surface is likely to be a lava ocean (Rouan, Deeg, and Demangeon 2011), reflecting the melting of rock and formation of a rock vapor atmosphere, which would occur under such conditions. Other notable planets included within this classification are CoRoT 7b, 55 Cancri e, and Kepler 78b (Howard,

Sanchis, and Marcy 2013). Studying these hot rocky exoplanets will contribute to the dataset needed to understand and model the evolution of planetary systems (Hu, Seager, and Bains 2013). In order to inform astronomical observations, experimental data from analog systems must be collected in the laboratory. Since the exoplanet environments cannot be directly sampled, modeling of observations using lab data will be the only means available to guide our understanding in the next several decades (Fogtman-Schulz et al 2014).

If the geometrical arrangement of the star, planet and earth are appropriate, light from the star can pass through the atmosphere of the planet and exhibit spectral features from that encounter. It has been shown (Seager 2000 and Madhusudhan 2012) that it is possible then to draw conclusions about the planet's composition, which then provides a piece of the puzzle for the evolution of the entire system.

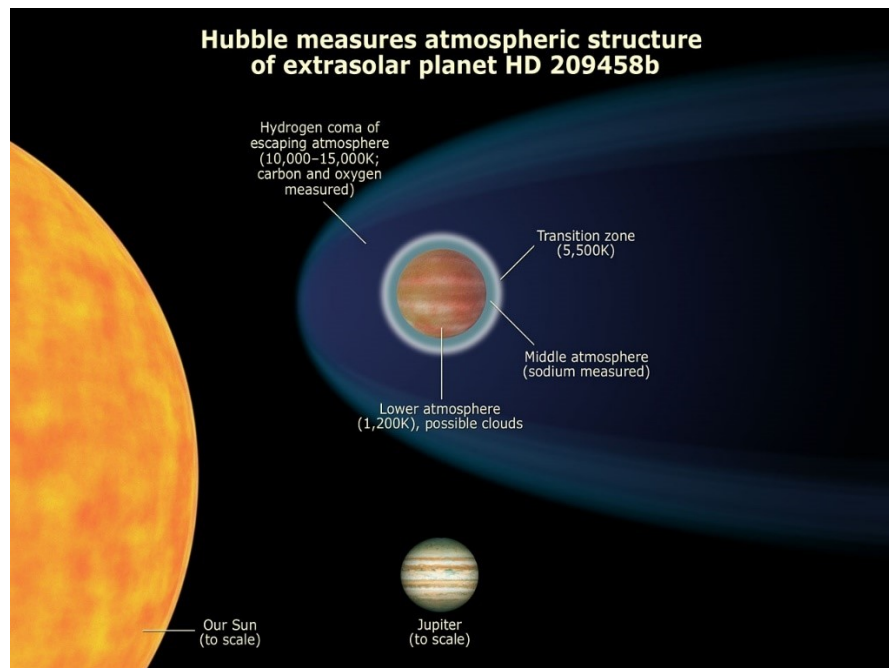


Figure 3. Showing HD 209458 off axis in comparison with Jupiter. (NASA, ESA, and A. Feild [STScI])

Atmospheres

Composition of the atmospheres of these previously stated extrasolar planets has been an issue of interest, but there are difficulties in extracting useful data from observations. Computational work is currently driving much of the insight. The models need both the general temperature and composition for the planet under investigation, and the thermochemical data for likely molecules. The general composition of the exoplanet is based primarily on its density. The density can be estimated using data obtained from two observations; radial velocity measurements of the shift in the star's light (used to find the mass of the extrasolar planet) and a transit of the exoplanet in front of its star (allowing its size to be determined). Radiative models of the stars and likely albedos for the planets are used to calculate the temperature of the planet, and for larger Jovian planets has been measured directly through the secondary transit of the exoplanet. The partial pressures of the gaseous constituents from the surface can then be computed. One such model is MAGMA developed by Schaefer and Fegley (Miguel et al 2011) for surface conditions greater than 1000 K. This code has been shown (Miguel et al 2011) to work with previously acquired Kepler data.

As mentioned earlier, an example of this kind of lava-planet is CoRoT 7b (Schaefer et al 2012). The dayside of this tidally locked planet reaches a temperature even higher than that for the previously discussed Kepler 10b. This permanent ocean causes sublimation of the Komatiite composition creating the rock vapor atmosphere. The composition of Komatiite can vary greatly and Figure 4 shows the atmospheric gas concentrations of a simulation under varied assumptions (Schaefer et al 2012).

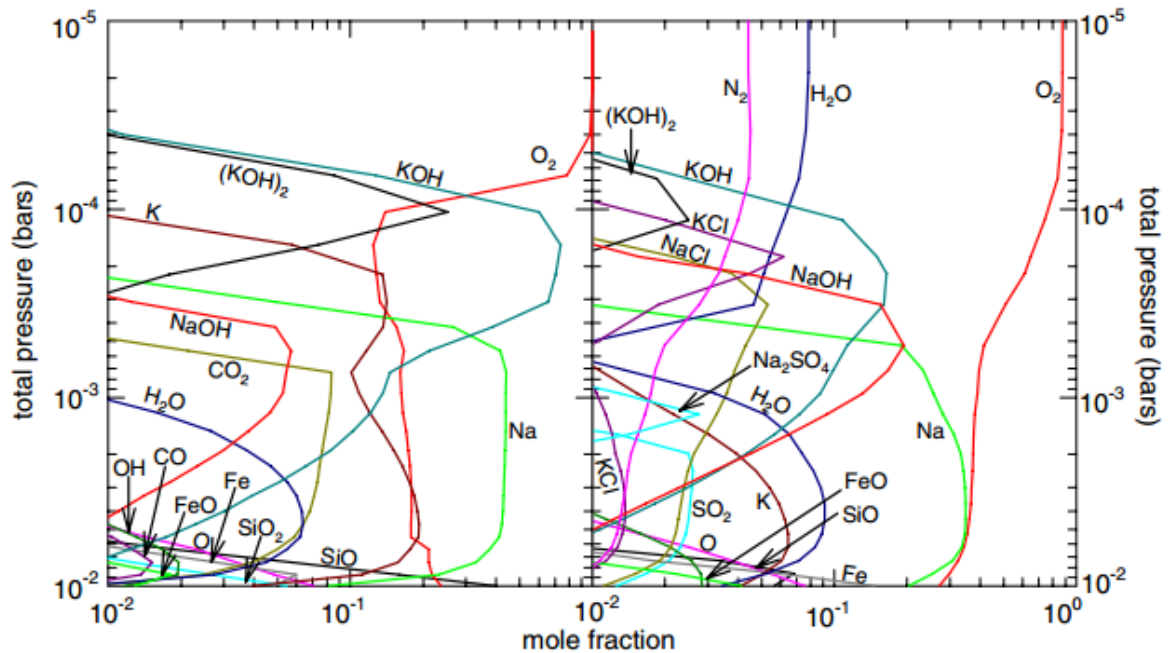


Figure 4. Atmospheric gas composition for CoRoT-7b assuming 2500 K temperature and 10-2 bar pressure for two alternate compositions, calculated using MAGMA (Schaefer et al 2012).

Once the modeling for the atmospheric composition of a planet is available, observational data must be obtained that allows comparisons to be made. A method which can provide data on elemental composition must involve E-M radiation stimulated spectroscopy in some fashion, which presupposes the presence of a light source. The method used is a variation on one of the primary detection methods for extrasolar planets, that of planet transiting, in which the planet passes in between its star and the line of sight to the earth. When the planet transits through the optical path to the star, a loss of light, as viewed from the earth, occurs, which is the way to detect the planet. In addition, one can view the refracted, transmitted light through the atmosphere of the planet. As well, when a planet passes behind the host star a secondary dip of the intensity of the light occurs. This dip in intensity can also be analyzed to determine atmospheric properties

(Seager and Sasselov 1998, Miller-Ricci Kempton, Zahnle, and Fortney 2012, Howe and Burrows 2012). These transitions are shown in Figure 5.

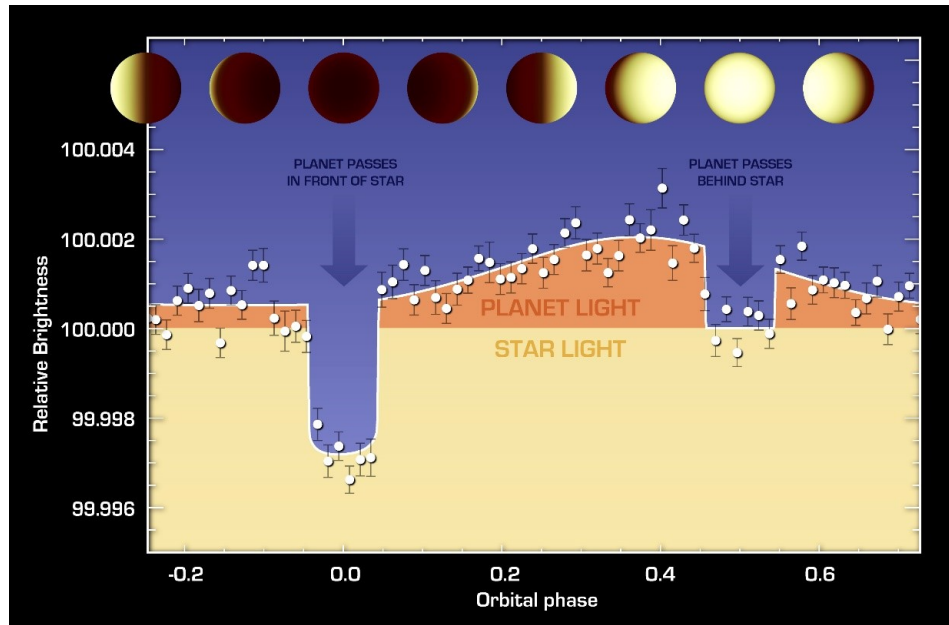


Figure 5. Showing the variation of brightness from both star and planet while in orbit of 55 Cancri e. (NASA/JPL - Caltech/University of Cambridge)

Observing the star through these episodes allows the extraction of spectral information from the transmitted light. This information can be directly related to the composition of the planetary atmosphere (Fortney 2016). A number of technical issues must be resolved for this technique to yield consistent and testable results (Fortney 2016). The primary issue is the small size of the signal contributed to the measured starlight from the interaction with the atmosphere (Martins et al 2013). For example, in the case of HD 209458 b, the ratio of the transmitted light to parent star light is 10^{-4} (Seager 2000). Within the atmosphere of the transiting planet, there are two typical components of interest, the optically thin and thick regions. Other points that must be considered are the refraction of the star's light through the atmosphere, the distinction between optically thin and thick portions of the atmosphere (Hu and Seager 2014 and Hui and Seager

2002), the presence of clouds and haze in the atmosphere (Fortney et al 2013) and the instrumental and systematic problems that arise from the observational techniques themselves (Fortney et al 2016).

As a simple explanation of the process, we examine the effect of gaseous constituents of the planetary atmosphere on the blackbody curve associated with the planet under examination. As shown in Figure 6, the blackbody curve is a depiction of the intensity vs wavenumber of the light emitted from the sun, before and after it has passed through the atmosphere of the earth. The molecules of the earth's atmosphere leave absorption features in the spectra, in much the same way (although more prominent) that light from a distant star will have features induced in its spectra by the atmosphere of its planets.

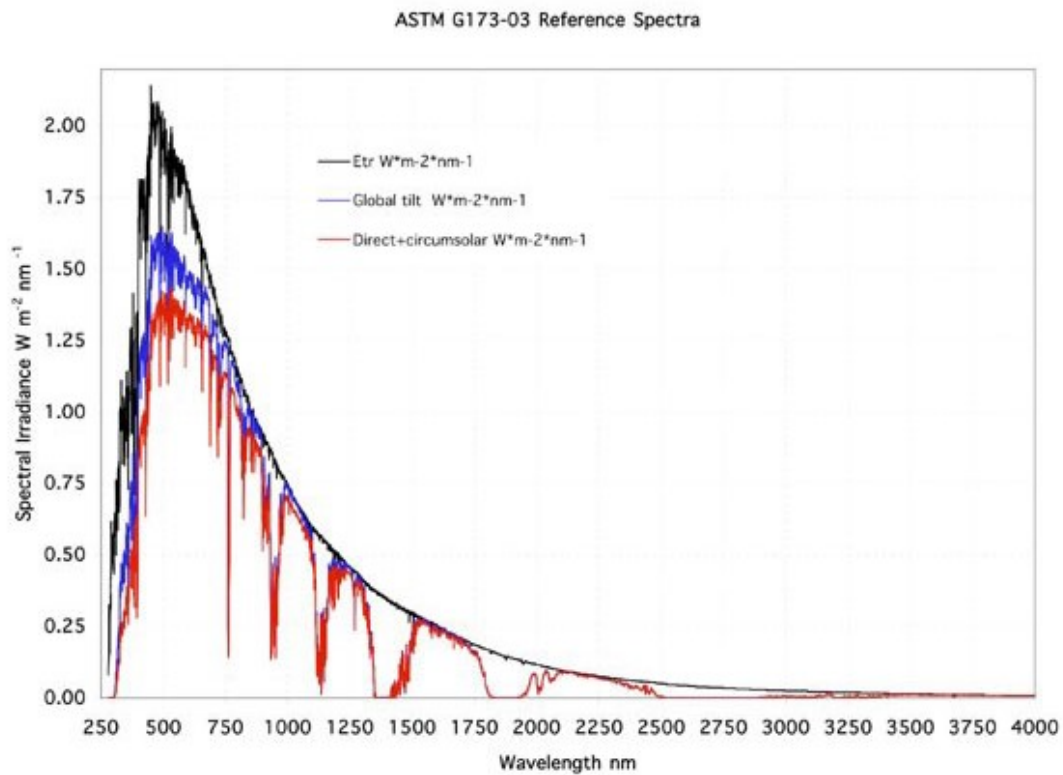


Figure 6. Spectrum of sunlight (black) and sunlight that has passed through Earth's atmosphere (red) (ASTM 2012).

The modeling or interpretation of spectra or photometry obtained using these techniques will depend, in great part, on the availability of data for known systems that might reflect the conditions of these exoplanets (Hu, Seager, and Bains 2012)

Lab Work

To fully exploit the observations being done and projected over the next ten years, especially through the using of the James Webb Telescope (Fortney et al 2013), one must have data for known systems. This data must come from lab work, and covers only a small part of the needed information (Fortney et al 2016). Especially lacking is data for hot systems, such as those for rocky planets at temperatures greater than 1500 °C (Fortney et al 2016).

In order to address the issue, first a device capable of producing the necessary temperatures had to be constructed. This device was an e-beam evaporator, capable of reaching 2000 °C (Bosch 2015). In this evaporator, I would place a crucible as part of an e-beam evaporator and evaporate samples using the well-known Knudsen Cell technique (Miller and Aramtys 2013). The evaporator is only the first item needed for a system, which must allow for the use of a full range of experimental techniques in the analysis of evaporated material. In earlier work (Bosch 2015), this system was proposed but it is the aim of this work to describe the engineering, construction and testing of the full system.

Using this system, I am now able to grow a sample of the evaporated material and perform infrared spectroscopy on the resulting molecules. Using a quadrupole mass spectrometer, the mass of the deposited molecules is also measureable. Additional information, including the temperature of the evaporator, can also be determined.

Throughout the remaining sections, the entire system and its application to the most basic of predicted hot exoplanets constituents, SiO, will be detailed.

THEORY

Fourier Transform Infrared Spectroscopy

The basic principles of Fourier Transforms allow one to convert measurements taken in the time domain to the frequency domain. I can use this tool to take an interferogram obtained from a spectrometer as a function of time and transform it into frequency space which is then associated to a blackbody plus absorption spectrum associated with the wavenumbers of light. The mathematical relationship is shown in the following form:

$$I(t) = \frac{1}{\sqrt{2\pi}} \int_{-\infty}^{\infty} G(\omega) e^{i\omega t} d\omega; \quad G(\omega) = \frac{1}{\sqrt{2\pi}} \int_{-\infty}^{\infty} I(t) e^{-i\omega t} dt \quad (1)$$

This is a powerful tool for the analysis of spectra, depending on the type of instrument used to acquire the data. In some spectroscopic instruments, such as a grating spectrometer, the light from the sample is dispersed by wavelength so the data as collected already show a spectrum. However, there are drawbacks associated with this method. In most lab work done currently, a device called a Fourier Transform Infrared Spectrometer (FTIR) is used. This acronym is just a fancy stand-in for a Michelson Interferometer, which is shown in Figure 7.

The FTIR creates an interferogram by inducing a phase difference between paths of a light source. This is done by sending a beam through a beam splitter bouncing one beam off of a stable mirror while the other bounces off of a moving mirror. This causes a phase difference as they come back together and are propagated through the system and in turn creating an interference pattern which becomes our interferogram, which is a function of time. The key point is that all wavelength data are gathered at once so the

speed of acquisition is usually enhanced (Smith 2011). As the beam passes through the sample material the associated wavelengths, correlating to certain wavenumbers, are absorbed. With some information removed from the light beam, the interferogram will change to reflect the lack of certain wavelengths. A numerical Fourier transform will then be performed on the interferogram and the spectrum as a function of frequency (or wavelength) calculated. The spectrum will have absorption features, as seen in Figure 8, corresponding to transitions in particular molecules. The number of photons absorbed by the material will correlate to how many molecules are present, depending on the strength of the transition. The transition strength for given molecules can be determined from other experiments or by calculation.

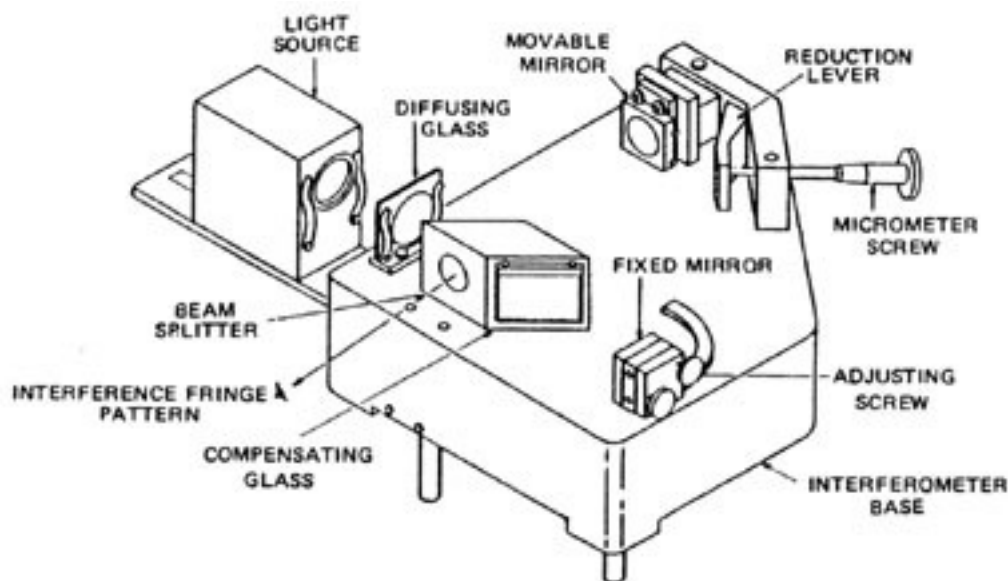


Figure 7. A Michelson Interferometer. (<http://pe2bz.philpem.me.uk/>)

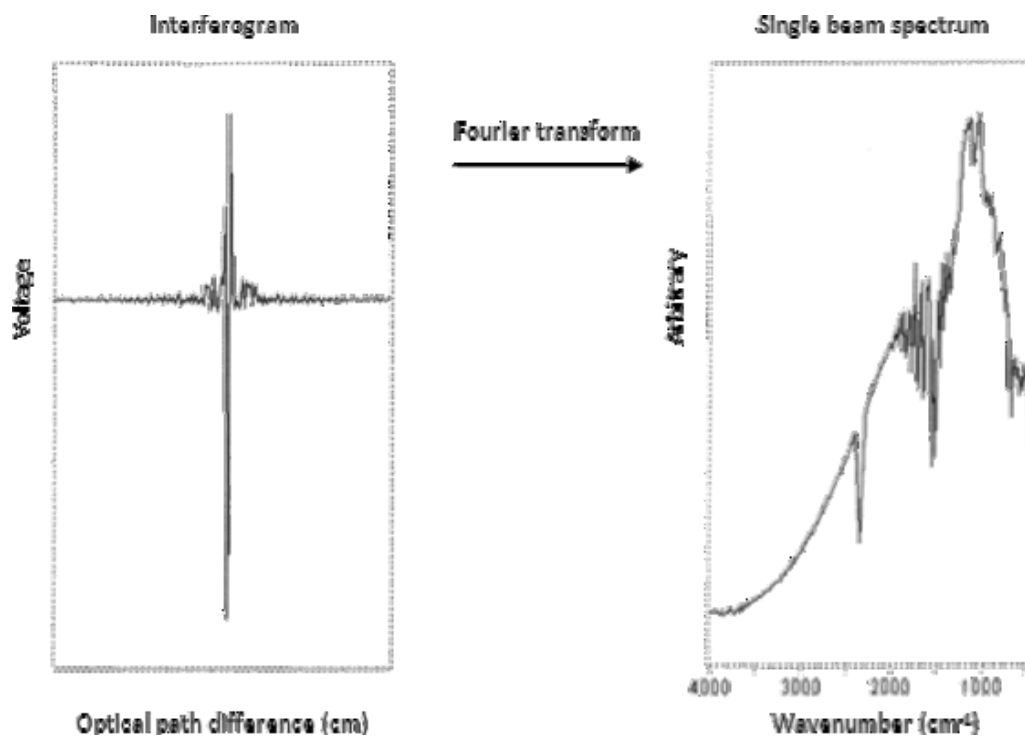


Figure 8. Graphical depiction of a Fourier Transform from frequency space to time space. (UC, Davis/ Jing Zhao)

Knudsen Cells

In order to use thermal evaporation as a way to study the environment of a planetary atmosphere, one must ensure that the technique approximates those conditions. It is essential that the temperature range be appropriate and, for the e-beam evaporator constructed earlier (Bosch 2015), the ultimate target temperature of 2000 °C is more than adequate. It is also important to remember that the environment of the planetary surface is in near equilibrium, at least in some local sense. Unfortunately, for a crucible with a large open top inside a vacuum environment (necessary for high temperature experiments), the system is not in thermal equilibrium. To attain an equilibrated state, one would require a closed system, where the vapor-liquid-solid system could come to its equilibrium as a function of temperature. The molecules produced must be sampled and so the compromise is that a small hole be put into the lid. When a crucible is used in

such a way, it is typically called a Knudsen Cell (Jacobson 2002), after the scientist who came up the technique.

In such a cell, the geometry must be such that the size of the orifice is small relative to the size of the container. Figure 9 shows such a cell, which must be constructed from a material resistant to the temperature. A refractory metal, such as Tantalum, is typically used. The material is chosen based on its melting point and resistance to oxidation (Hannay 2012 and Shukla et al 2004).

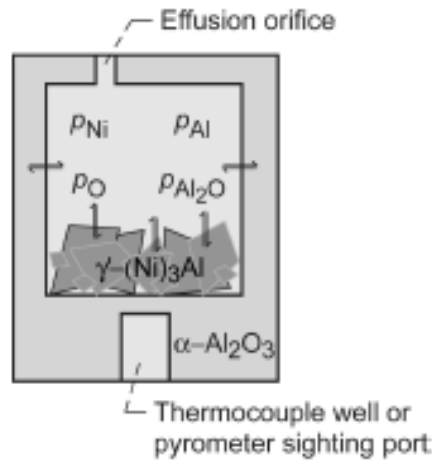


Figure 9. Depiction of Knudsen Cell. (Copland and Jacobson 2010)

The flux of material from the orifice of the cell can be calculated using kinetic theory (Carlson 1967) and is given by the equation

$$\frac{dN}{dt} = A_0(2\pi mk_B T)^{-\frac{1}{2}}(P^* - P) \quad (2)$$

Where P^* is the equilibrium pressure of the evaporant, P is the ambient pressure working against evaporation, and A_0 is the cross-sectional area of the orifice. If the orifice is not a pure surface, but is instead a finite length the flux must be multiplied by the Clausing

factor W_c , which is the proportion of incident flux that escapes due to the shape of the orifice (Jacobson 2002). For an ideal orifice, molecules exit the orifice according to a cosine distribution. A deviation will occur if the orifice is non-ideal. Using the geometry established between the Knudsen cell and the sample collection area, the number of detected molecules determined by the FTIR analysis can be related back to the rate of escape at the orifice and then to the vapor pressure for a given starting mixture and temperature (Akishin 1967).

Matrix Isolation

Even though the evaporator will provide a sample of the gas-phase molecules in equilibrium with the contents of the Knudsen cell, the molecules must be put into a position where they can be observed. While in the cell observation is impossible and, as a molecular beam within the vacuum chamber, the molecules are too tenuous to provide a measurable signal. It is possible to deposit the effusion material onto a flat substrate and measure the IR signature, but the result would be applicable to a solid-state film and not to individual gas-phase molecules. To overcome this obstacle, I rely on the standard technique of matrix isolation spectroscopy. Essentially what this technique attempts to achieve is to isolate a certain system in a state similar to that of the gas phase. This is advantageous to me because the molecular beam created from constituents being evaporated within the crucible is quite small as in the given number of molecules per unit volume is not high. Therefore, while I could attempt to send the IR beam through the evaporating constituent beam the technique wouldn't be able to distinguish the interaction from that of the noise. I use this technique to solve said problem.

With the establishment of a ratio of 1000:1 of the matrix elements to evaporate elements, the matrix can isolate the evaporates and “freeze” them in their native state. (Bally 2004) Another requirement directly follows, as there cannot also be interaction between the evaporates and the molecules creating the matrix as well as the interaction between the evaporates and IR beam (Nakayama et al 2012). The first causing molecules not representative within the crucible and the second creating noise making the evaporate signal non-distinguishable.

Therefore, I have chosen the noble gas, Argon, to be the matrix element. It is both inert and unresponsive in the infrared spectra. In order to create a matrix of Argon, the cryostat must cool down our target or flag to less than 20 K. This allows the Argon to be frozen in a specific form and not aggregate. This also will limit aggregation of the evaporants.

ENGINEERING

Chamber Design

The initial work, or proof of concept, was done in a cylindrical chamber. This chamber had many limitations. One major limitation was the inability to make FTIR measurements as the evaporation was occurring. Others stemmed from the port availability and locations for many desired devices such as an interferometer, gas inlet, and others. I solved this problem with the design of a spherical chamber. The chamber allowed one to have many optically connected ports, meaning one could bounce a beam in and out of the chamber, which allowed for simultaneous measurements. Also, the chamber has allowed us to have more flexibility for placement of our ion gauge, turbo pump, gas inlet, mass spectrometer, interferometer, e-beam evaporator, IR thermometer, and cryostat.

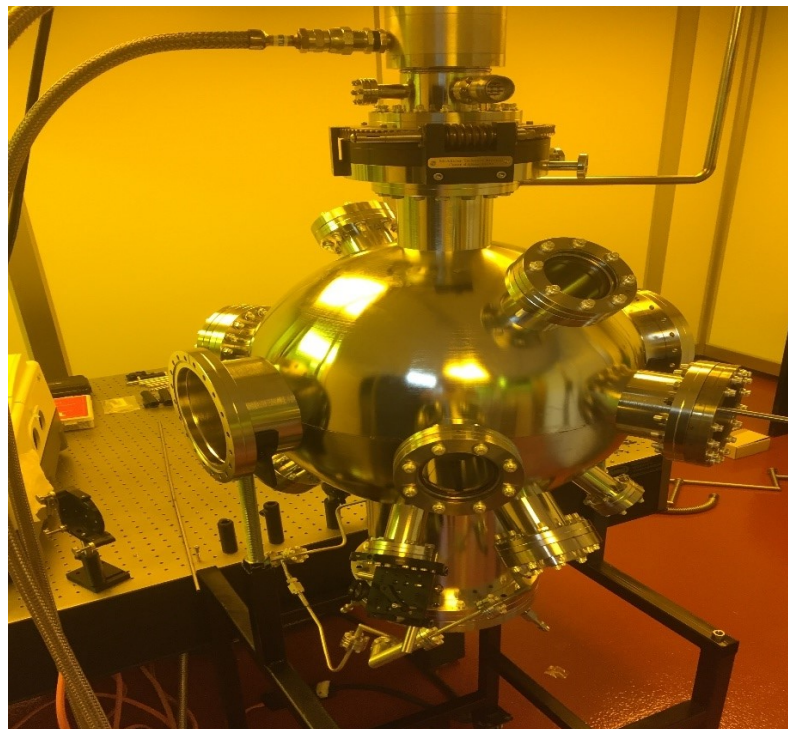


Figure 10. Spherical chamber in process of building set up. (Heath Gemar)

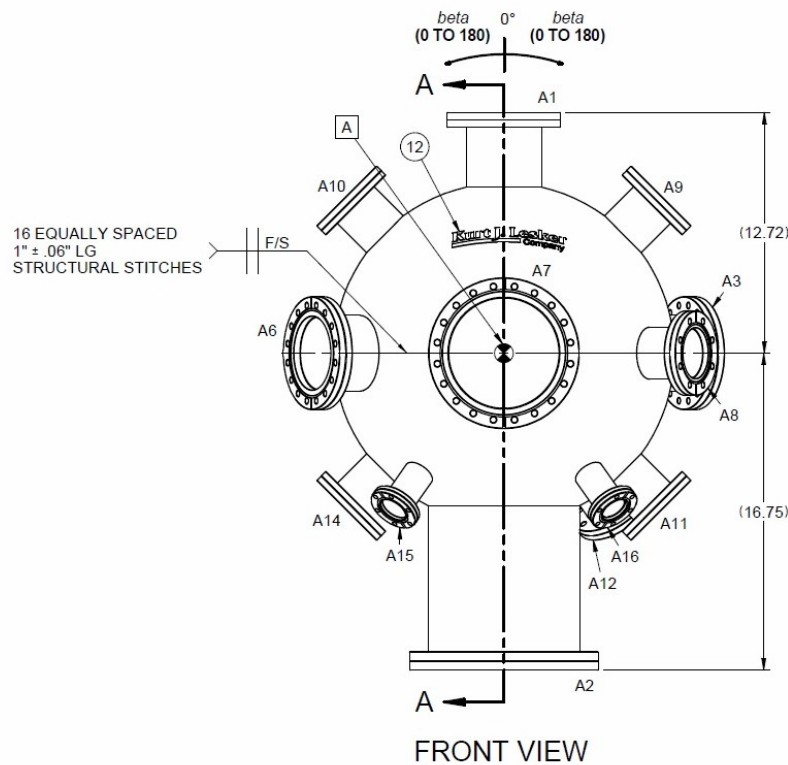


Figure 11. Spherical CAD design. (John Lester)

The new chamber was able to achieve ultra-high vacuum. I used a rotary vane pump to achieve a rough vacuum to 10^{-2} Torr of pressure. After this I used a turbo molecular pump to achieve much lower pressures. With the additional help of baking the chamber using heating tape I was able to achieve chamber pressure of 10^{-10} Torr.

E-beam evaporator

The initial work and design of the e-beam evaporator used was done by Denny Bosch (Bosch 2015). I was able to eliminate three of the six supporting rods and reduce the number of platforms from three to two in the original system. These changes helped reduce deposition rates to achieve closer to the matrix isolation requirements, which I

will detail later. To better control the heating and cooling of the system, a program was written which is explained in the engineering results section.

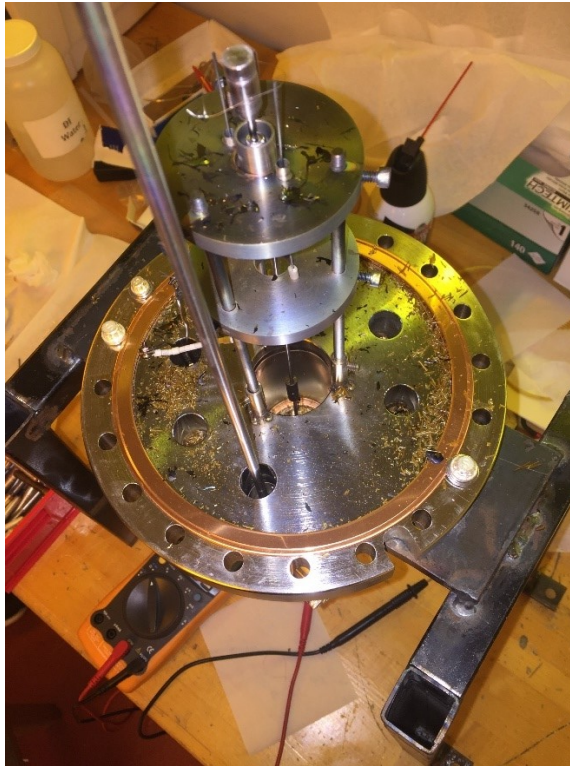


Figure 12. E-Beam Evaporator post-run. Flakes are cooled SiO fallen from cooling shroud. (Heath Gemar)

In addition, I was able to add a cooling shroud around the evaporator. This helps prevent further contamination throughout the chamber while also creating a sharper temperature gradient throughout the chamber.

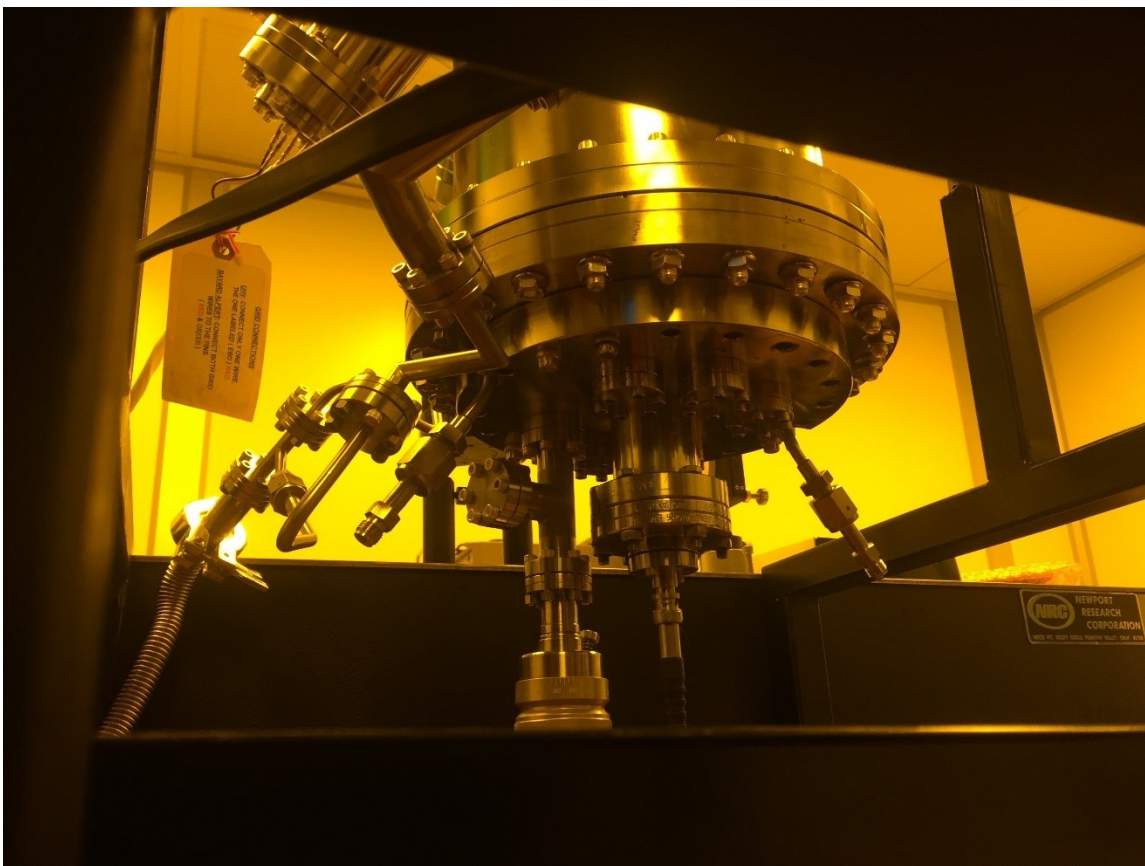


Figure 13. Cooling shroud and shutter set up from underneath the chamber. (Heath Gemar)

Another addition to the evaporator was installation of a shutter in front of the evaporator. This allowed me to shut off the evaporation without reducing the temperature, figure 12. An advantageous use of this system was also found during degassing. This device allowed me to eliminate many highly reactive gases such as nitrogen and hydrogen without depositing our rocky material from the crucible.

IR Optical Path

I additionally acquired an optics table for our FTIR system. This table allowed one to position the mirrors in such a way so that our parabolic mirror used to focus the beam was the proper distance to maximize exposure. Also, the set-up allowed

optimization of the beam into and out of the chamber for measurements. The light was first emitted from the source, bounced off of a 3" gold plated mirror, a gold plated parabolic mirror, and then from our 2" Gimbal mounted gold-plated mirror into the chamber at a 45-degree angle. Gold surfaces were used on each optic due to its enhanced reflectivity.

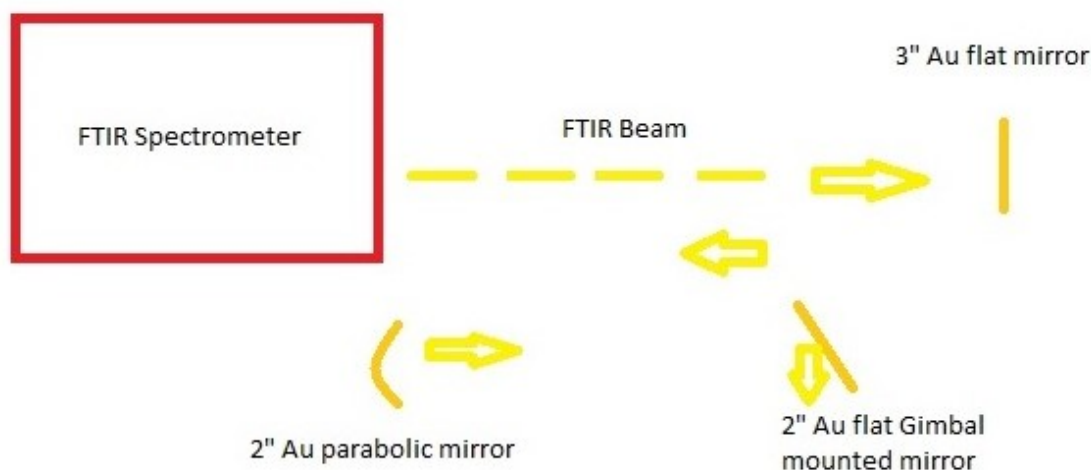


Figure 14. Optical pathway going into the chamber from the IR source. (Heath Gemar)

In order to reflect the beam out of the chamber, the sample and Ar matrix must be grown on a mirrored surface, which makes thermal contact with the cryostat. A special solid copper (for thermal properties) mirror with $\lambda/15$ surface roughness was used and is shown in Figure 15.

Because the beam exited the chamber at a deflection of 45 degrees, I used another Gimbal mounted gold-plated mirror to re-orient the beam parallel with the detector plane. From here I bounced once off of a flat gold-plated mirror, into another parabolic mirror, and finally focusing into our detector connected to the FTIR system.



Figure 15. Copper mirror used as flag within the system. (Michal Bulak)



Figure 16. Optical pathway exiting the chamber. (Heath Gemar)

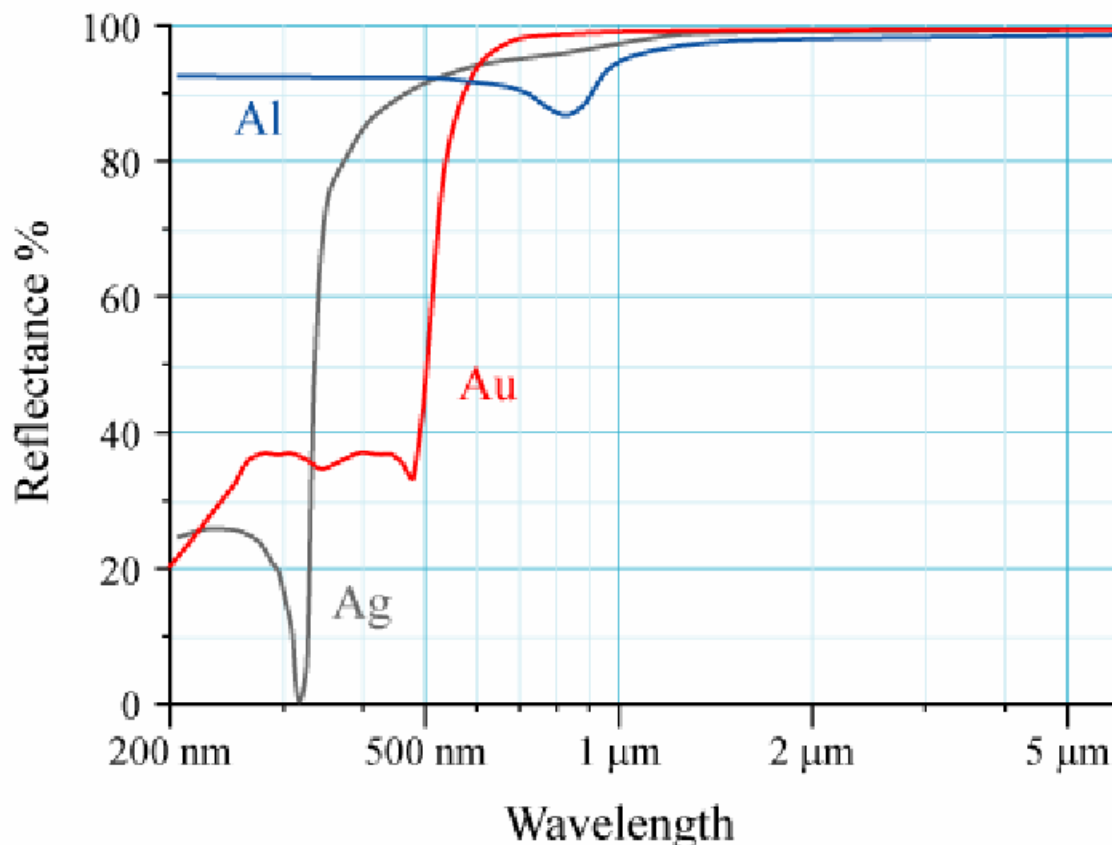


Figure 17. Graphical representation of Au, Al, and Ag as a function of wavelength. Showing Au to be the best choice for mirrors given our wavelength. (Bob Mellish)

Thickness Monitor

As described earlier, while growing the matrix, the Ar to evaporant ratio must be 1000:1. In order to ensure this it is necessary to measure the Ar ice thickness during each experiment. To do so, I built an interferometer using a laser diode as a source, a photo diode as a detector, an operational amplifier, and a computer interface system (Labjack and LabVIEW). The laser diode was connected to the chamber via a 2.75" port adapter with multiple posts and 90 degree connectors allowing for 3-dimensional manipulation. On another port 180 degrees separated from the laser port I attached a photo diode in similar fashion while also placing a 1" lens in front to focus the beam onto the detector.

From here I attached the photo diode to a current-to-voltage amplifier. I used a Labjack to read the voltage amplification through the computer.

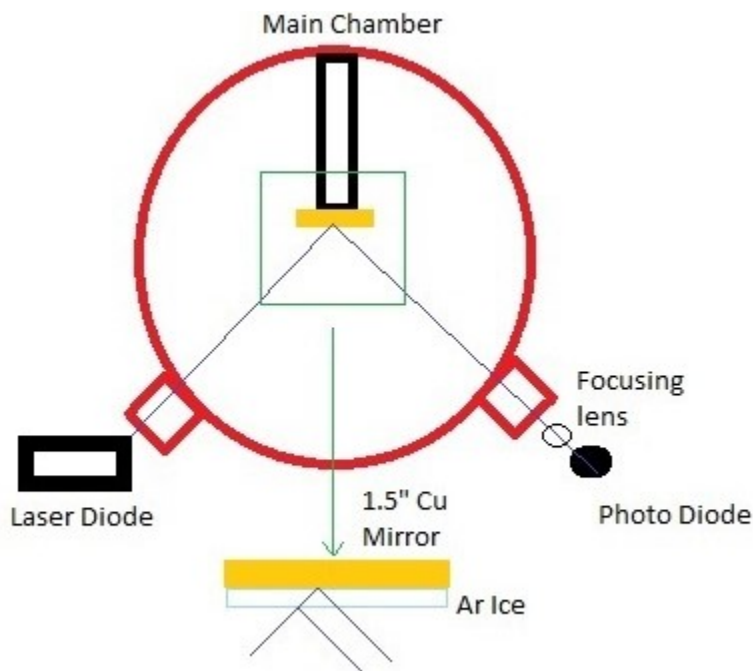


Figure 18. Optical pathway of the thickness monitor. Depiction of where the path difference occurs. (Heath Gemar)

Future direction with the interferometer would require the installation of a beam splitter on both the input and output with a second laser and photo diode. This would allow one to determine the refractive index and the thickness of the ice.

Gas Inlet

In order to establish a proper Argon matrix, I needed to develop a gas inlet system that not only would create a uniform film at a high enough rate but one that would stay out of the two separate optical pathways. I decided to proceed in two directions: one direction being a ring sitting outside the mirror with a radius of 3" and many holes, all of the same size, pointed in the direction of mirror (Figure 18) and the other being a ring

sitting at the level of the mirror with four individual prongs branching down bending into the 1.5" radius of the mirror (Figure 18 and 19).

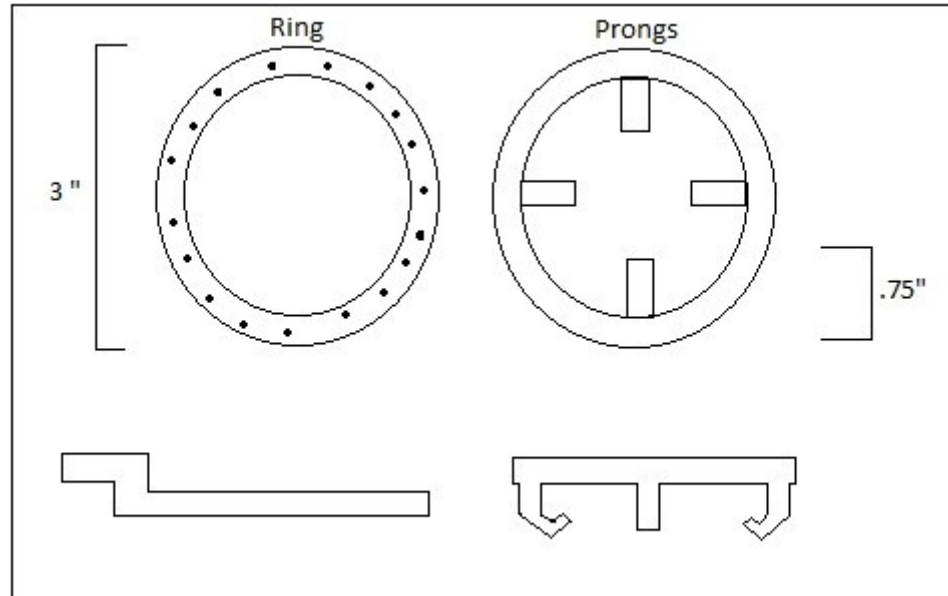


Figure 19. Depiction of the two separate gas inlet designs. The left having a series of holes while the right has a series of tubes leading to the center. (Heath Gemar)

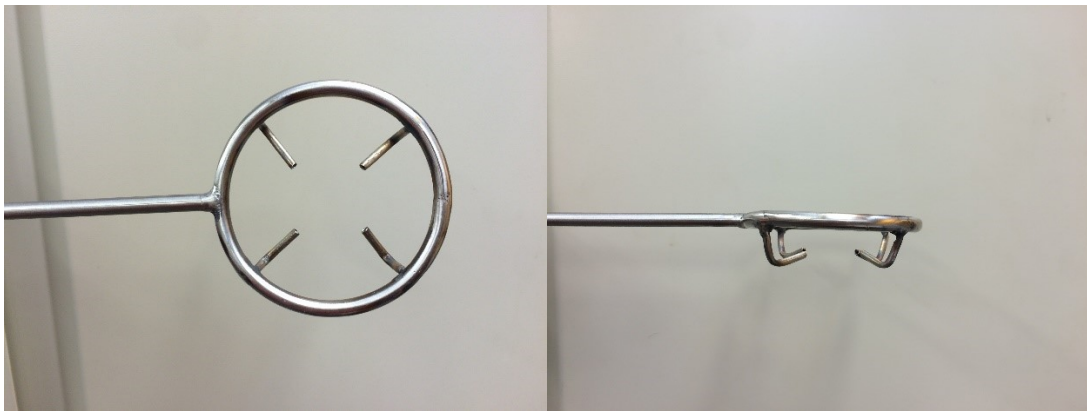


Figure 20. Picture of actual prong gas inlet. (Michal Bulak)

The resulting deposition rates will be discussed and shown later within this thesis. Refer to the Engineering Results for further reading. The Prong design as depicted in Figure 19 and 20 is the design that gave us a higher deposition rate.

Thermometry

I used an IR thermometer of wavelength 0.65 microns to determine the temperature of the crucible. I was able to do this through a 2.75" port on the top side of the chamber. The transmission loss through the quartz window was negligible. I also cut an access through the top of the cooling shroud to have a straight-line view of the crucible. As an aside, I discovered we had a small amount of material being sent through the secondary hole and very slightly coating the window with material. To correct for this obstruction, I cleaned the window between every run as to reduce the transmission loss to the negligible amount previously stated.

Using an infrared thermometer requires one to know the emissivity of the material. The emissivity for many materials changes only a slight amount over a wide temperature range. However, tantalum's emissivity shows a larger variation, requiring a correction to accurately read the thermometer. This process is described in the engineering results section.

EXPERIMENTAL

With a circumferential filament I was able to remove the crucible without disturbing the e-beam evaporator. I cleaned the crucible by sonicating in acetone. Then, I would tare the crucible and add sample which would be SiO₂ from Supelco Analytical, MgO from Sigma Aldrich, Opal (hydrated SiO₂) from Missouri State University's Geology Department, and a combination of SiO₂ and MgO. I would then remass the crucible containing the sample. I closed the chamber with our sample inside using copper sealed conflat flanges. I would then start the rotary vane pump to establish a chamber pressure less than 3×10^{-2} Torr which in turn allowed us to use the molecular turbo pump and establish a pressure of 1×10^{-9} Torr. From here I would take a 'warm' background spectra of the clean flag, copper mirror finish. In preparation for the matrix isolation, the cryostat was engaged, which would drop the temperature of the copper mirror to 15 K. In response, the chamber pressure would drop to the low 10^{-10} Torr as some remaining volatiles were cryo-pumped. Once our flag was sufficiently cool, I would take a second background to take in any slight variation which may have occurred with the blackbody diagram. Following this I would flood the chamber with argon through our gas inlet system using a sapphire leak valve, establishing a chamber pressure of 3×10^{-6} Torr. Before evaporation, the interference of the argon ice was monitored from our blue laser and photo diode and a layer of a few microns was grown to protect the mirror of any evaporant that may occur unknowingly from our crucible. After a sufficient amount of Argon was deposited I would take another background to examine any more shifts in the blackbody diagram. I would then monitor our mass spectrometer and discontinue ramping as both the filament and crucible would outgas hydrogen gas, nitrogen gas,

oxygen gas, and water. While monitoring the crucible with our IR thermometer and checking the level of emission current produced we would wait until the desired temperature was reached and open the shutter while continuously taking FTIR spectra of the flag. I would then close the shutter and allow the control program to slowly ramp down the crucible to room temperature. Once sufficiently cooled we would close our argon leak valve. After the evaporation, we continued to acquire FTIR spectra to monitor for reactions induced by the diffusion of reactants throughout the ice. When all was completed we would turn off the compressor and allow the flag to warm back to room temperature.

Some complications occurred with various crucible designs. These complications centered around lid fitting and the clogging of the orifice during deposition. I eventually settled on an all tantalum crucible drilled by Missouri State University machinist Brian Grindstaff. We also used the services of Jonathan Keeth to laser puncture an orifice in our lid ranging from 0.1 mm to 0.5 mm.

PROGRAMMING RESULTS

LabVIEW

In order to have a higher degree of control, I elected to operate our power supplies for both the crucible and filament through the computer. LabVIEW allowed me to have the desired controls of reading the emission voltage and current (crucible) as well as reading and writing to the filament voltage and current. Because of this program, I was also able to regulate the ramping rates (both up and down) occurred. As described in the experimental section, the program was used to ramp, control, monitor and cool down the evaporator.

Along with the power supplies, I used LabVIEW to read the analog output of the IR Thermometer. The thermometer works by assuming an emissivity and focusing through a reticle. However, the emissivity of the tantalum crucible changes as a function of temperature. Therefore, I create an emissivity curve based on the NIST database of tantalum's emissivity at specific temperatures. I have this detailed in the engineering results section. From this, I was able to establish a given equation to autocorrect the analog signal to correct for this problem of changing emissivity and read correctly in the program. I was also able to read the global pressure of the chamber through the analog out from the ion gauge. The voltage drop needed for the interferometer as detailed in the engineering and theory sections was also read through the Labjack.

All of this data was stored and maintained in a text file for archive purposes. This proved useful while troubleshooting and getting the system up and running so that certain major factors were taken into account.

Omnice

The program used to control our FTIR spectrometer was Omnic. Within this program, preset macros can be utilized to control the FTIR. Therefore, I wrote a macro to continuously save spectra as well as save them in a file setting that could be instantly analyzed within the Matlab program I wrote to do fitting and extraction as I will detail in the Matlab section.

Matlab

Another need of our group was the need to analyze a large amount of spectra efficiently and coherently. Therefore, I wrote a program to accomplish such a task. The code was designed, so that based on desired examination regions defined by the user, to examine if there was or was not a peak and determine its position, height, area, and fit to a desired background. The program accomplished this task by stripping the data for the ranges desired. It then would take the natural log of the ratio of the background to signal. From here, based on the shape of the resulting graph would determine whether or not there is a peak corresponding to a real feature. The background was typically of higher intensity than the signal collected during the run. This is due to various scattering effects through the growth of the Argon ice. Because of this, I had the program fit the peak and find its range. From here, the program then fit the line to minimize the noise in the signal. From here the area, height, and peak position were able to be obtained directly. The program would then store this data and display them in the graphs you can view in the Scientific Results section of this thesis. After being done with all the ranges of interest throughout all of the individual growth spectra collected, it would display the time

progression of all main parameters analyzed. This code is written out in detail in the appendices of this thesis.

Other programs written through Matlab for use in our laboratory accomplished the following functions: reanalysis of any data set, quick data lookup through a database everyone in the research group contributed to building, emissivity corrections, and various geometrical analysis for design purposes dealing with optical pathways and construction of elements.

ENGINEERING RESULTS

Gas Inlet

I performed a series of measurements with use of the interferometer to determine the amount of growth of ice on the copper mirror. I would allow the compressor to run fully, dropping the temperature of the mirror to 15 K. At this temperature, the gas that was chosen for use in this project, argon, freezes. I was determining a growth rate that would at least give us a ratio of argon molecules to evaporate materials of 1000 to 1. It was necessary to adjust to approximately this ratio in order to prevent frost formation as this would cause scatter of the incident light. Below are figures detailing the interference patterns observed.

The rate of deposition was increased by a factor of 4.7 from the ring to the prongs. The deposition rate was 2.31 microns per hour for the rings and 10.86 microns per hour for the prongs while chamber pressure was held at 3×10^{-6} Torr. Figures 20 and 21 show the interference patterns obtained with strictly growing an argon ice.

Emissivity

According to the NIST database correlating the temperature of Ta to emissivity, I have plotted these points and established a second order fit, Figure 23.

Emissivity: [.14 .19 .26 .30]

Temperatures (Celsius): [727 1093 1982 2930]

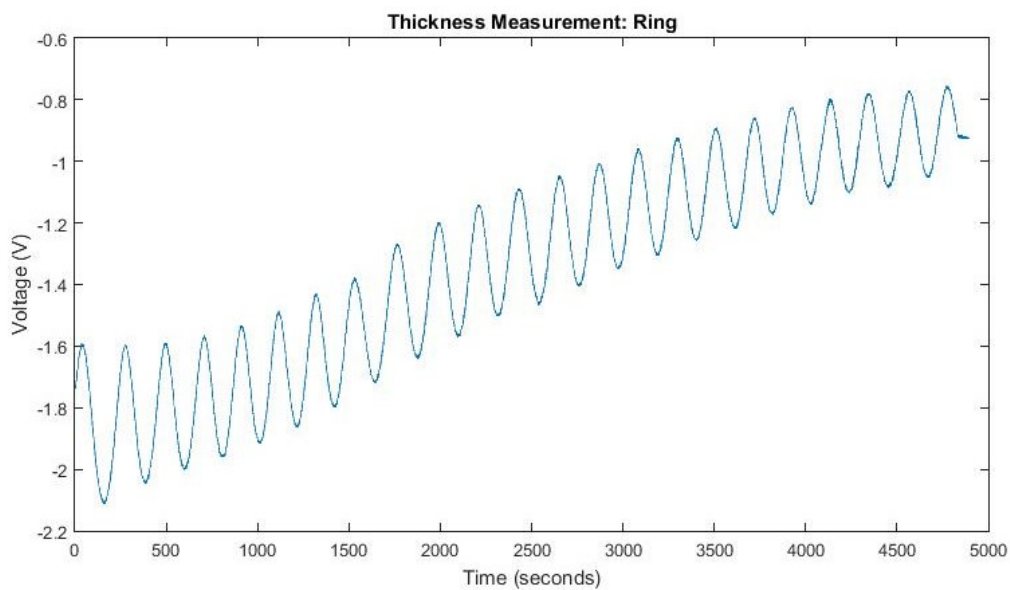


Figure 21. Interference pattern showing the growth rate of Ar ice using the Ring system at 3×10^{-6} Torr.

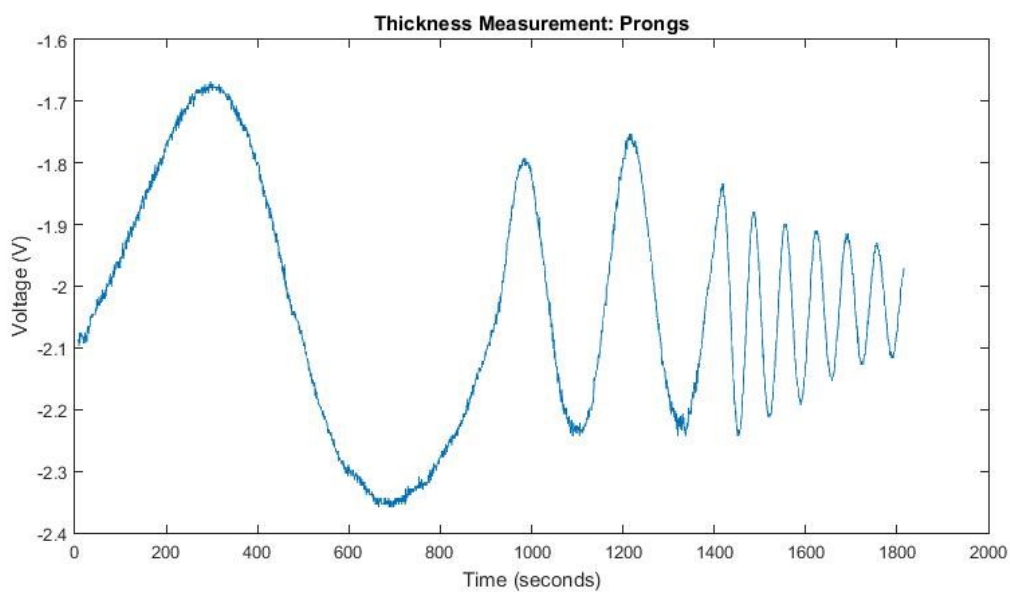


Figure 22. Interference pattern showing the growth rate of Ar Ice using the prong system at 3×10^{-7} , 6.7×10^{-7} , and 3×10^{-6} Torr.

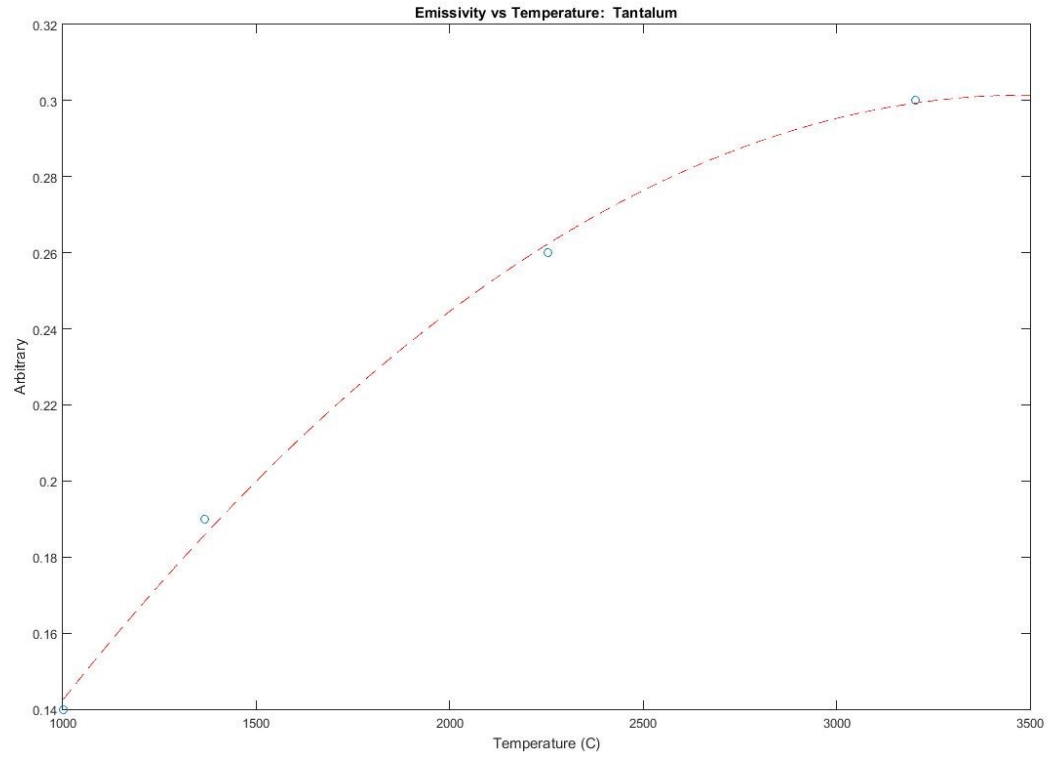


Figure 23. Graph showing the curve fitted to NIST data on Ta emissivity change with temperature.

Now I have the Emissivity values for any temperature from 1000 to 3000 C. I determined the temperatures relevant to our experiment, 1100 to 2000 C. Use of a 1 C step size and determined the emissivity for each temperature based on the previously shown curve.

Another portion of the situation is the power being detected and emitted from the crucible.

$$P = (\text{geometric factor}) * \epsilon * T^4 \quad (3)$$

The power emitted (P_e) from the crucible and detected (P_d) in the thermometer over the same geometric factor are equal. Therefore, I can set the power of both equal.

$$\epsilon_e * T_e^4 = \epsilon_d * T_d^4 \quad (4)$$

I know ϵ_d , as this is the setting I dictate on the thermometer (0.18). Because the emissivity (ϵ_e) values for any given temperature (T_e) is known, I only have one unknown: T_d which is the temperature that will be displayed on the thermometer. Now I can determine what each T_d will be for our range of T_e (Temp of crucible) we desire. I then plotted these values as shown in Figure 24.

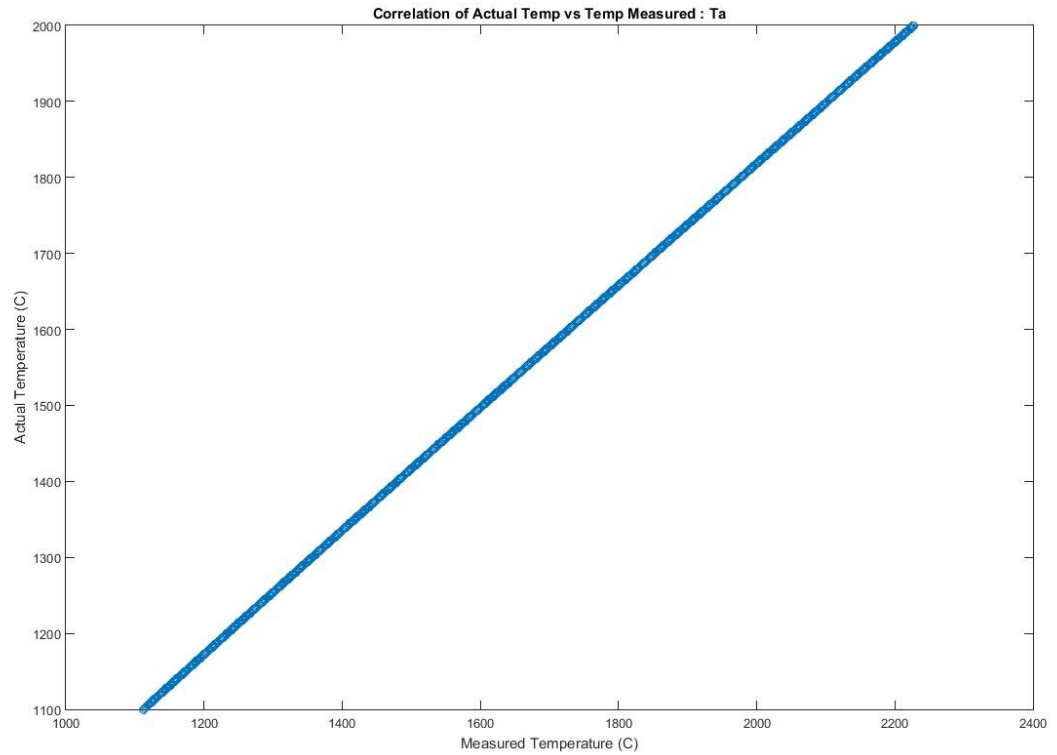


Figure 24. Graph showing the relationship between the measure temperature and true temperature as explained through the text.

I now have a linear correlation of Actual Temp vs. Measured Temp. I can now immediately correct for the wrong emissivity value on the thermometer and therefore determine the true temp.

SCIENTIFIC RESULTS

I have used the FTIR Spectra retrieved while heating the crucible using the e-beam evaporator at 1600 C. The data are described by an exponential term; therefore I have taken the difference between the spectra by dividing the background by the event spectra and taking the natural log of the ratio. These spectra were analyzed using the Matlab code developed as described in the CODES section. The first molecule to develop was the monomer SiO followed by the dimers and trimers, Si₂O₂ and Si₃O₃, respectively. As seen in comparisons between figures 24 through 41, the trimer (figures 36-41), dimer (figures 30-35), and monomer (figures 24-29) become more selective in said order. Growth 4 occurs 10 minutes after 1600 C has been achieved with Growth 5, 6, 7, and 8 being another multiple of 10 minutes after. After Growth 8, the shutter was closed and e-beam evaporator ramped down.

SiO

The following figures represent the spectrum collected and analyzed for the molecule SiO. The peak position corresponding to SiO is 1226 +/- 0.7 cm⁻¹ wavenumber. This is confirmed through the literature with peaks being observed at 1229 cm⁻¹ (Hastie) and 1225 cm⁻¹ (Journal of Molecular Spectroscopy). The slight shift in these lines is most likely due to scattering effects through the argon gas matrix. Citing the Journal with the theoretically accepted value, I have seen the corresponding condition within the spectrum.

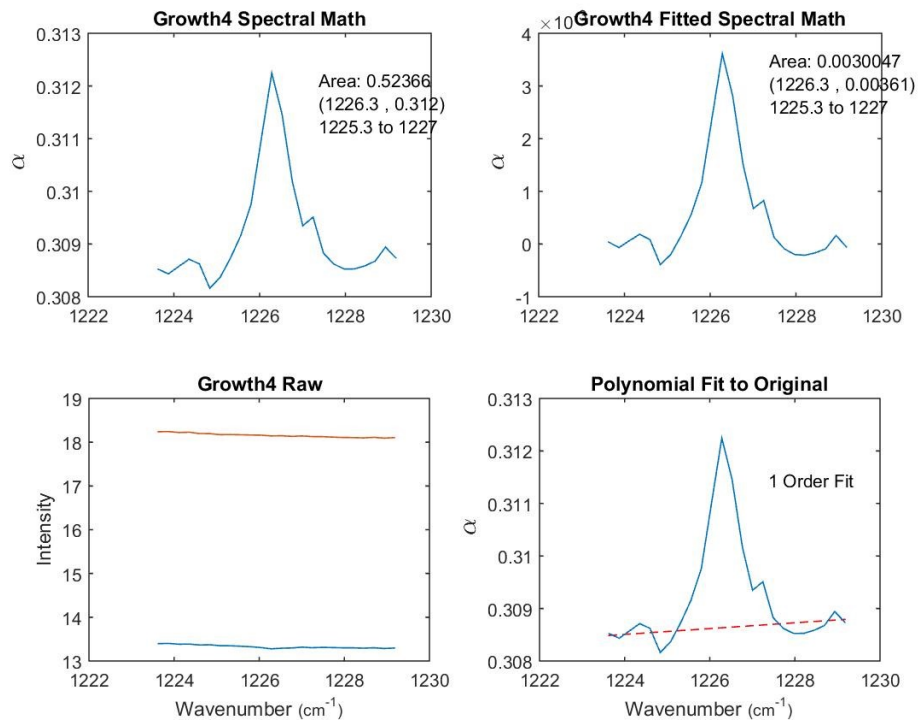


Figure 25. Use of the Matlab code developed to analyze the IR spectra observed. SiO peak 10 minutes after the shutter was opened at 1600 C.

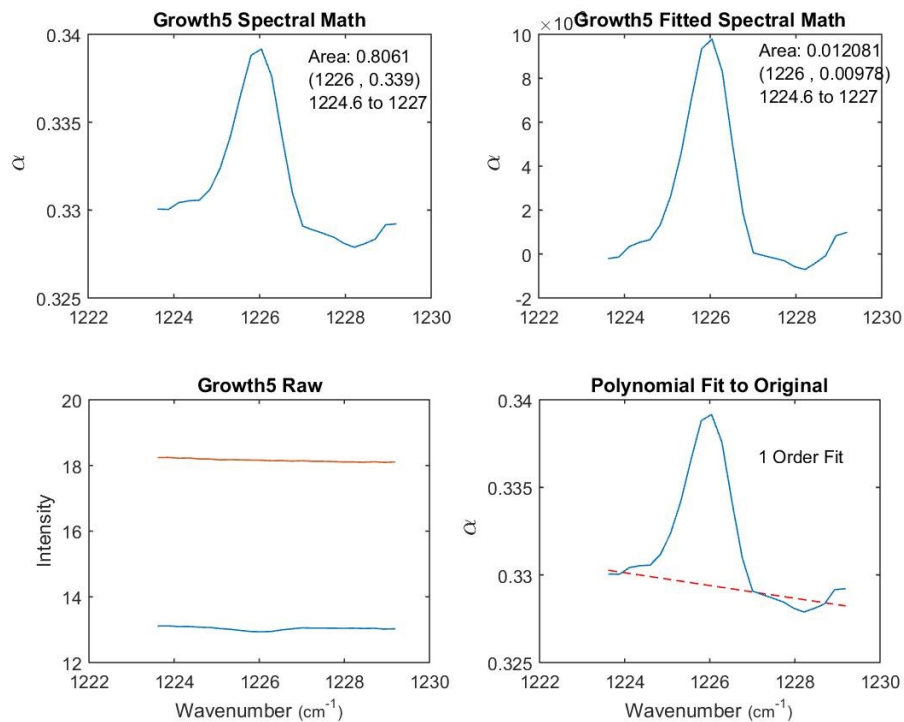


Figure 26. Use of the Matlab code developed to analyze the IR spectra observed. SiO peak 20 minutes after the shutter was opened at 1600 C.

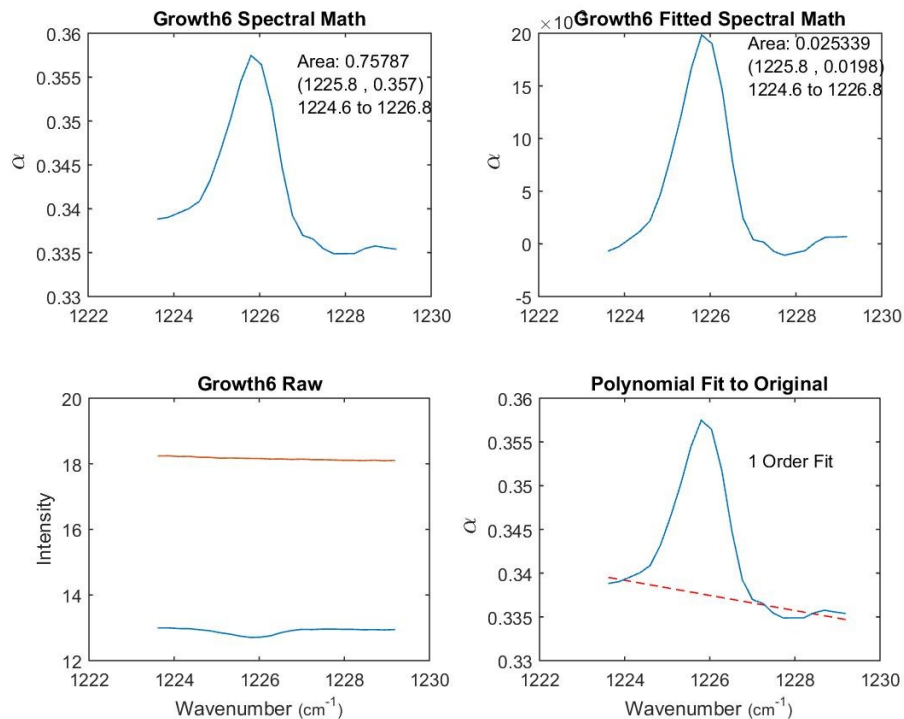


Figure 27. Use of the Matlab code developed to analyze the IR spectra observed. SiO peak 30 minutes after the shutter was opened at 1600 C.

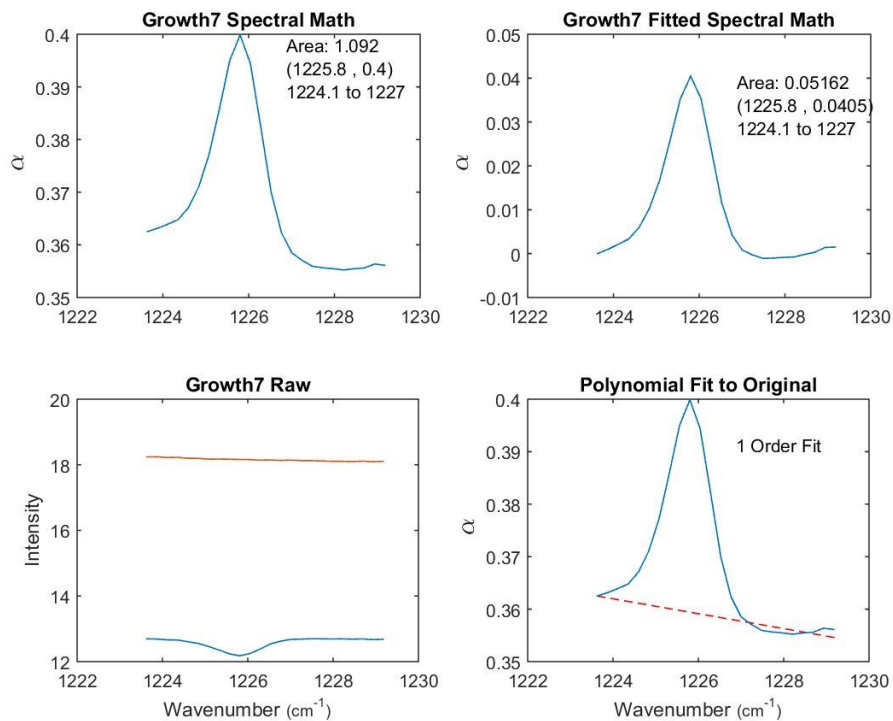


Figure 28. Use of the Matlab code developed to analyze the IR spectra observed. SiO peak 40 minutes after the shutter was opened at 1600 C.

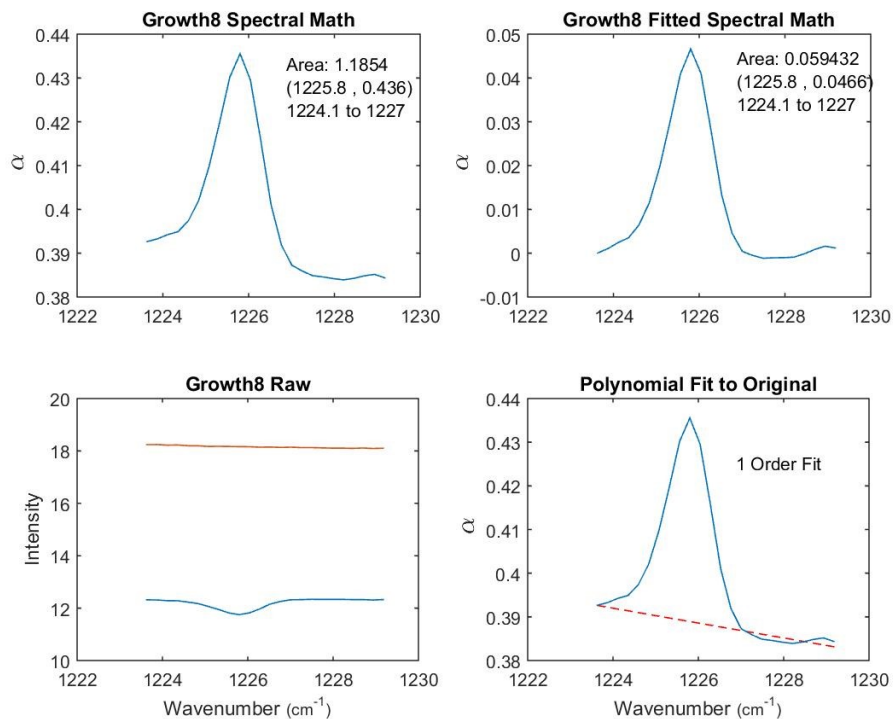


Figure 29. Use of the Matlab code developed to analyze the IR spectra observed. SiO peak 50 minutes after the shutter was opened at 1600 C.

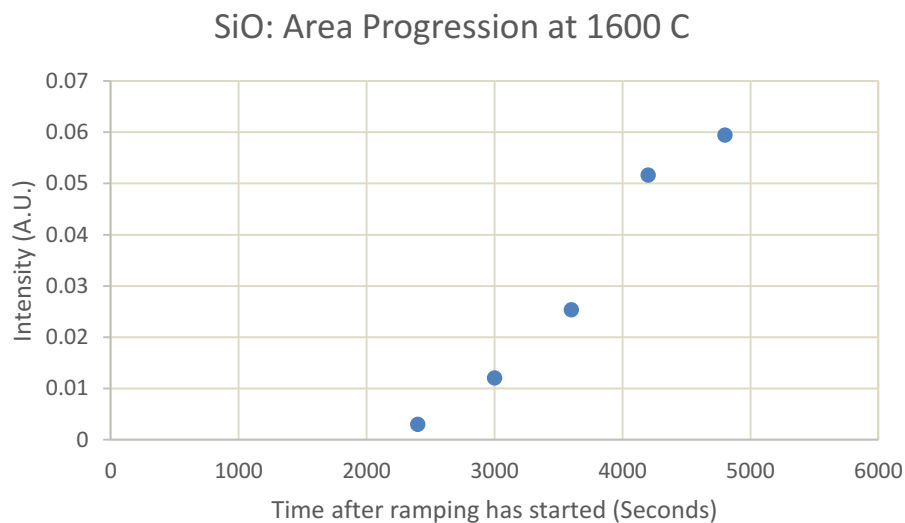


Figure 30. Graphical depiction of the Area Progression of the main SiO peak. Shutter was open and depositing for 50 minutes at 1600 C.

Si₂O₂

The following figures represent the spectrum collected and analyzed for the molecule Si₂O₂. The peak position corresponding to Si₂O₂ is 802.98 +/- 0.1 cm⁻¹ wavenumber. This is confirmed through the literature with peaks being observed at 802.9 cm⁻¹ (Journal of Molecular Spectroscopy). The slight shift of the argon matrix to the SiO lines did not appear to affect the Si₂O₂ as greatly. With the Journal being the theoretically accepted value, I have seen the corresponding condition within the spectrum. However, I note that within the first 10 minutes this molecule did not appear within our spectrum.

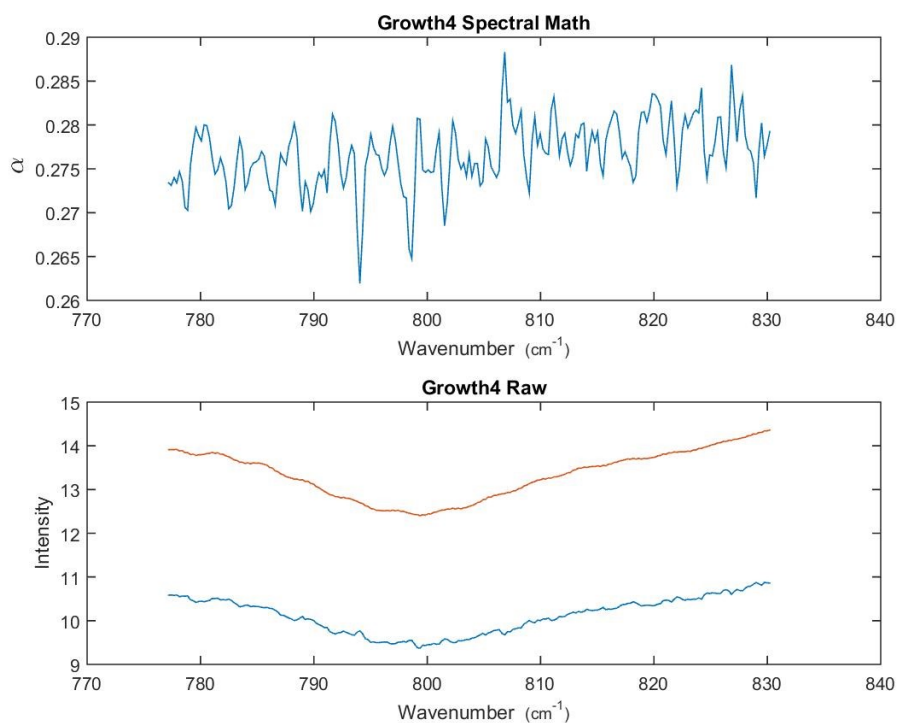


Figure 31. Use of the Matlab code developed to analyze the IR spectra observed. Si₂O₂ peak 10 minutes after the shutter was opened at 1600 C. There was no evidence after this amount of time that any Si₂O₂ was deposited.

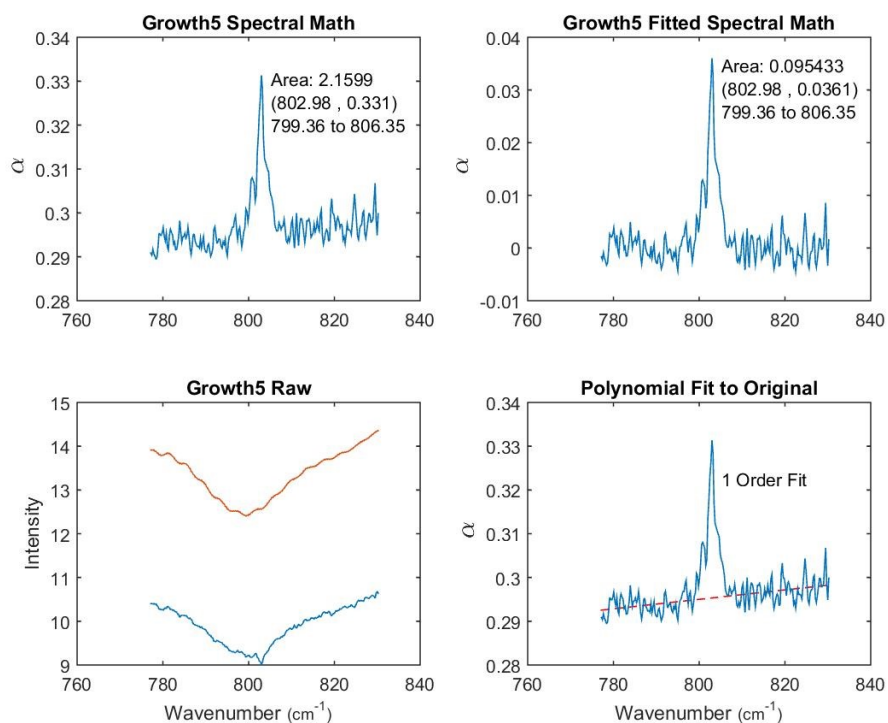


Figure 32. Use of the Matlab code developed to analyze the IR spectra observed. Si_2O_2 peak 20 minutes after the shutter was opened at 1600 C.

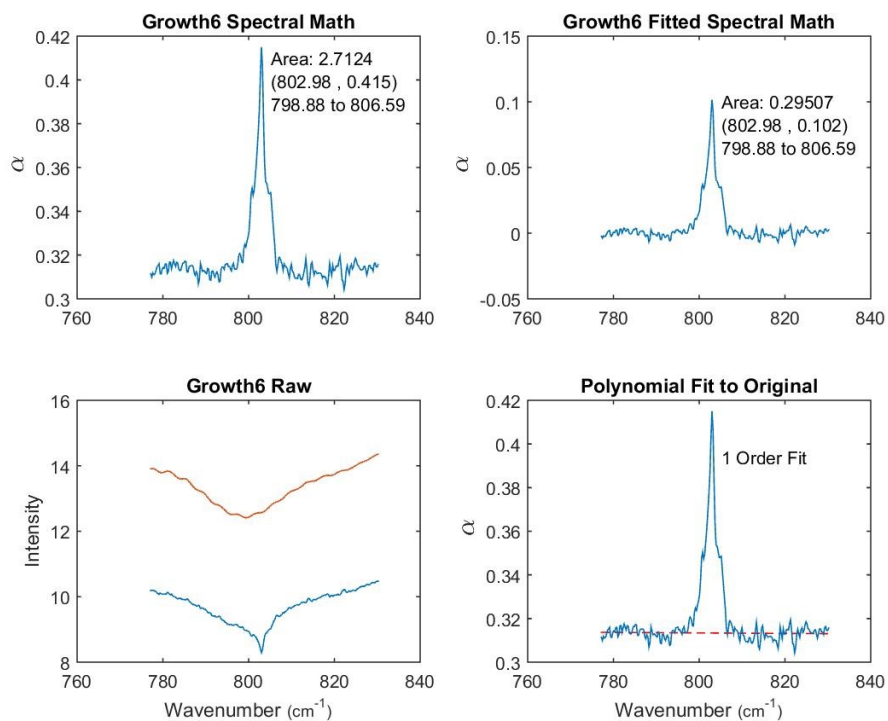


Figure 33. Use of the Matlab code developed to analyze the IR spectra observed. Si_2O_2 peak 30 minutes after the shutter was opened at 1600 C.

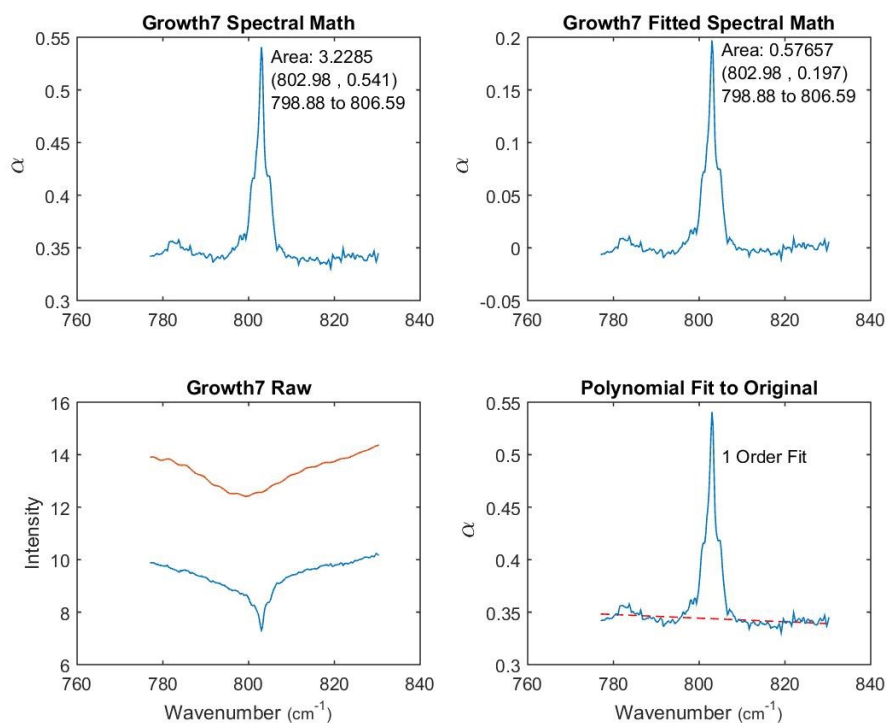


Figure 34. Use of the Matlab code developed to analyze the IR spectra observed. Si₂O₂ peak 40 minutes after the shutter was opened at 1600 C.

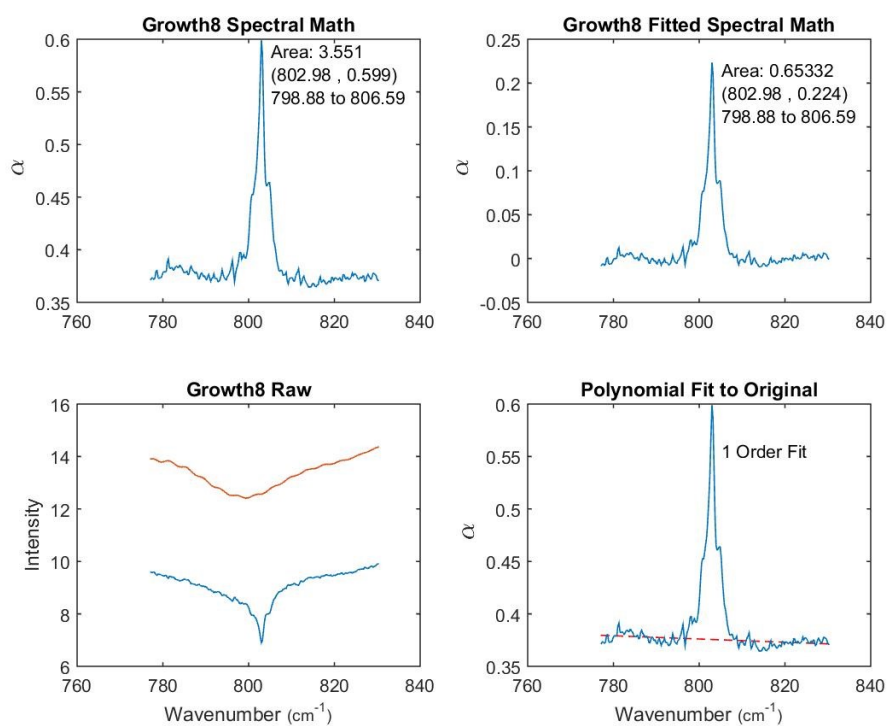


Figure 35. Use of the Matlab code developed to analyze the IR spectra observed. Si₂O₂ peak 50 minutes after the shutter was opened at 1600 C.

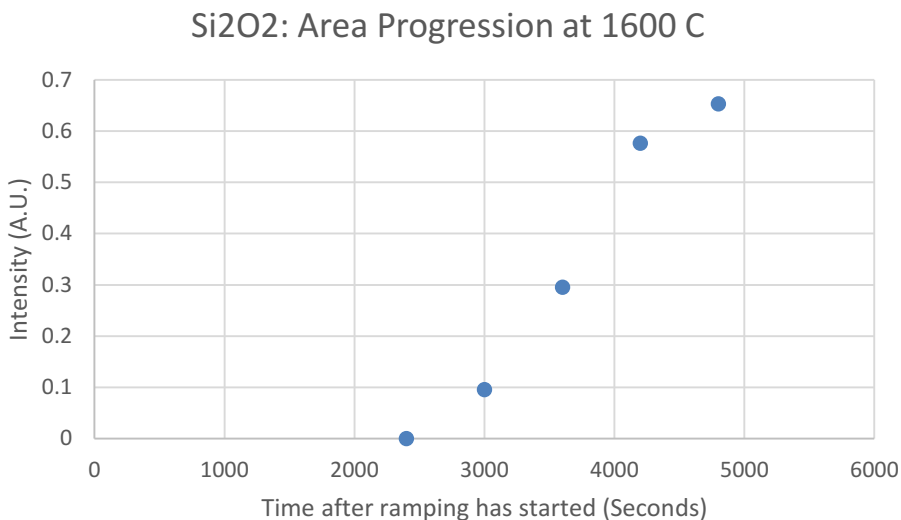


Figure 36. Graphical representation of the area progression of the main Si₂O₂ peak for 50 minutes at 1600C.

Si₃O₃

The following figures represent the spectrum collected and analyzed for the molecule Si₃O₃. The peak position corresponding to Si₃O₃ is 972.2 +/- 0.1 cm⁻¹ wavenumber. This is confirmed through the literature with peaks being observed at 971.0 cm⁻¹ (Journal of Molecular Spectroscopy). I again, like with SiO, have a further shift of the observed peak within the argon ice matrix. With the Journal being the theoretically accepted value, I have seen the corresponding condition within the spectrum. Similar to the Si₂O₂ molecule, I note that within the first 10 minutes this molecule did not appear within the spectrum.

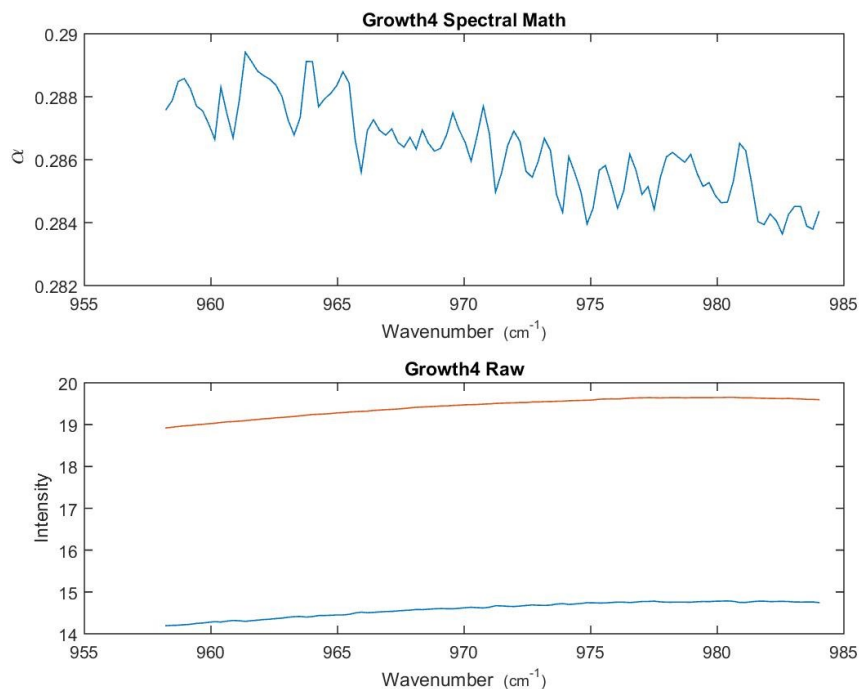


Figure 37. Use of the Matlab code developed to analyze the IR spectra observed. Si_3O_3 peak 10 minutes after the shutter was opened at 1600 C. There was no evidence after this amount of time that any Si_3O_3 was deposited.

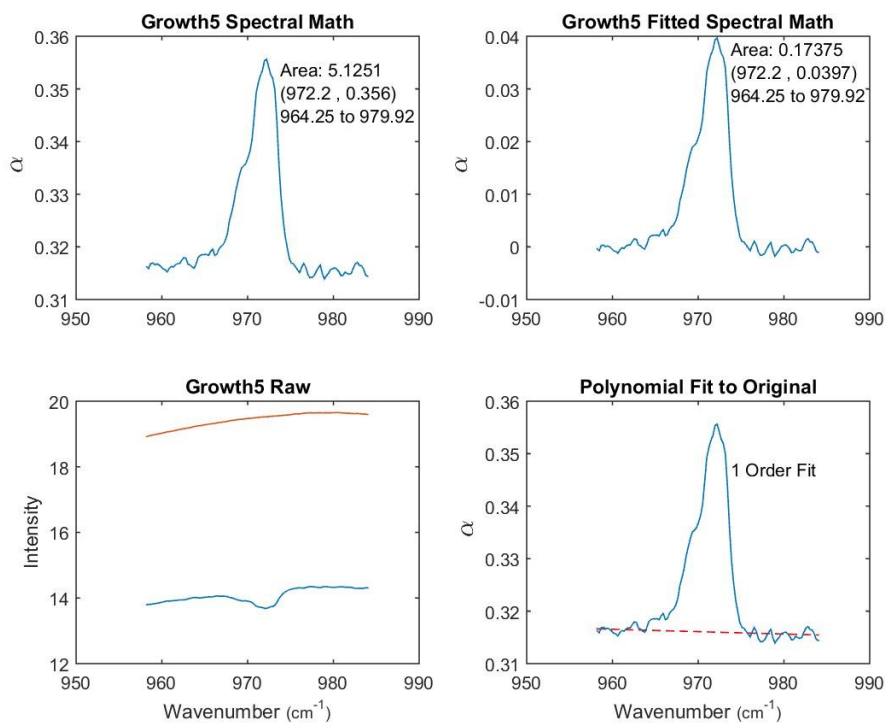


Figure 38. Use of the Matlab code developed to analyze the IR spectra observed. Si_3O_3 peak 20 minutes after the shutter was opened at 1600 C.

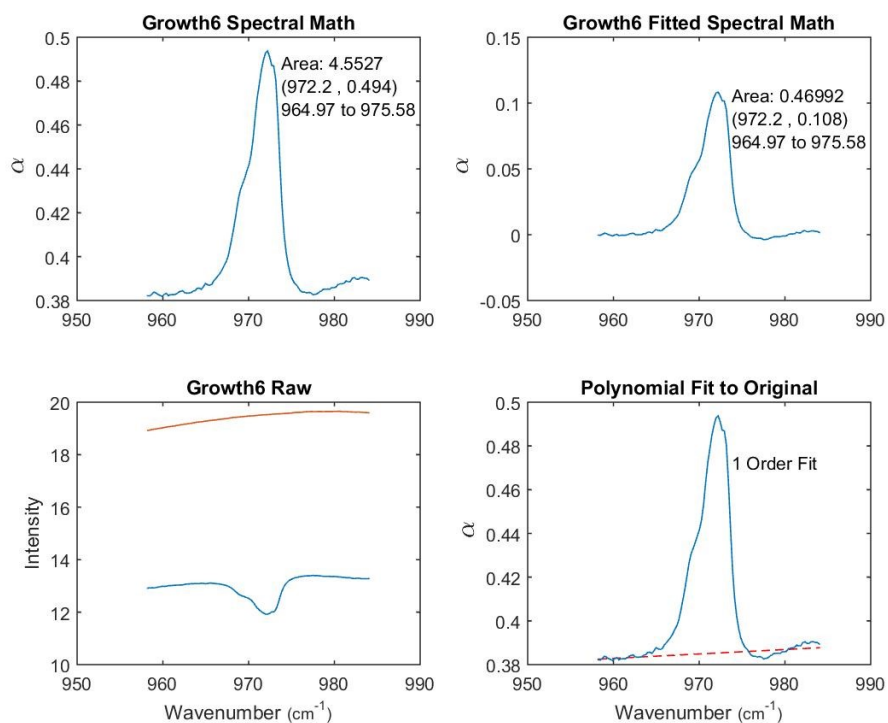


Figure 39. Use of the Matlab code developed to analyze the IR spectra observed. Si_3O_3 peak 30 minutes after the shutter was opened at 1600 C.

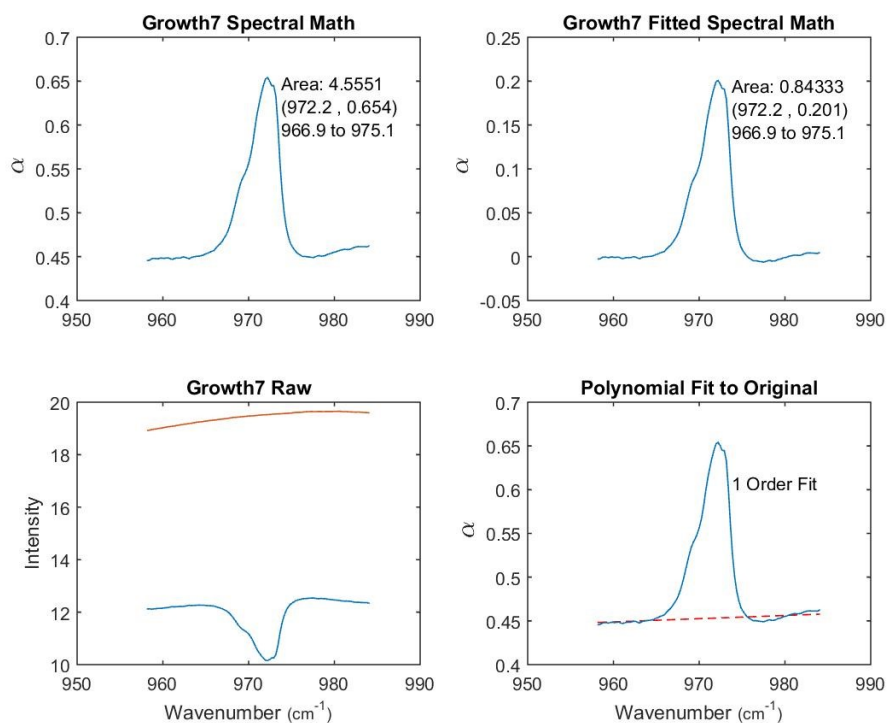


Figure 40. Use of the Matlab code developed to analyze the IR spectra observed. Si_3O_3 peak 40 minutes after the shutter was opened at 1600 C.

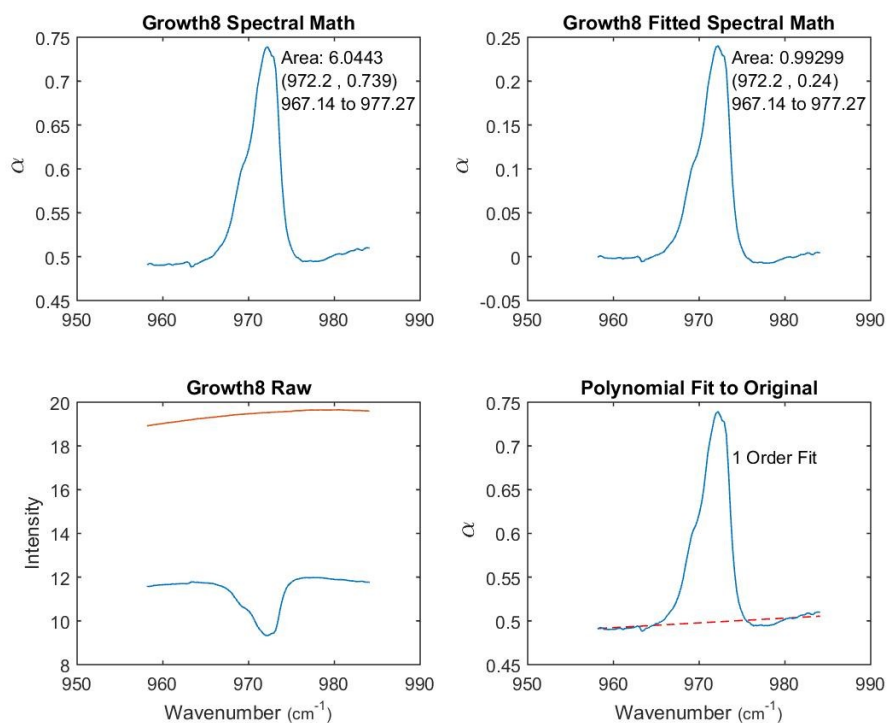


Figure 41. Use of the Matlab code developed to analyze the IR spectra observed. Si_3O_3 peak 50 minutes after the shutter was opened at 1600 C.

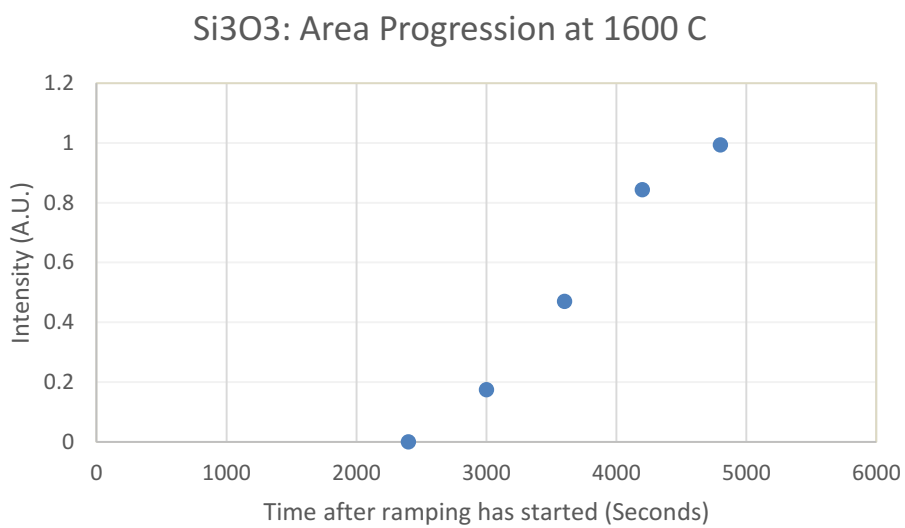


Figure 42. Graphical representation of the area progression of the main Si_3O_3 peak for 50 minutes at 1600C.

DISCUSSION

The timing of occurrence for the spectral features appear to follow the literature with the monomer being the first to appear, the dimer second, and the trimer third. However, under closer examination the intensities appear to grow in strength with trimer, dimer, and monomer being the order of strongest to weakest. This intensity variation is unlikely since, at 1200 °C, SiO should continue to be the most predominant species as shown through thermodynamic calculations by Dr. Sakidja. This discrepancy is most likely due to either a misfit with our crucible lid, or to the interaction of the molecules inside the matrix after deposition. In the case of the crucible, I must work through engineering concerns especially with lid tightness. This process will take several iterations to complete. The possibility of diffusion within the ice can be reduced by lowering the temperature of the matrix, which requires improvement in the cryostat currently being used.

Also, another avenue that will be pursued is the mixture of complex molecules going forward. One such combination is that of Al_2O_3 and SiO_2 which would create an IR active molecule SiAlO . Study of this could lead to some insight of how combinations of molecules affect the resulting spectrum.

With regards to the analyzing technique developed with the high volume of data, I have shown that I was able to take the information collected and verify with literature the silicon+oxygen molecules that were formed in the system. Further steps will require more information on peak area and its correlation to the actual number of molecules present in the sample. If one is able to determine this, one could use this as a guide for real world area inspection of FTIR spectrum.

REFERENCES

- Akishin, P. A. 1967, in *The Characterization of High Temperature Vapors*, ed. J. L. Margrave (Wiley)
- Armitage, P. J. 2010, *Astrophysics of Planet Formation* (Cambridge)
- ASTM G173-03(2012), *Standard Tables for Reference Solar Spectral Irradiances: Direct Normal and Hemispherical on 37° Tilted Surface*,
<http://rredc.nrel.gov/solar/spectra/am1.5/>
- Bally, T. 2004, in *Reactive Intermediate Chemistry*, ed. R. A. Moss et al. (Wiley)
- Bosch, Yarden, “Design of High Temperature Evaporator for Spectroscopic Study of Equilibrated Vapor Phase Materials” (2015). MSU Graduate Theses. Paper 1609.
- Carlson, K. D. 1967, in *The Characterization of High Temperature Vapors*, ed. J. L. Margrave (Wiley)
- Copland, E. H., Jacobson, N. S. 2010, NASA Report, NASA/TP-2010-216795
- Elkins-Tanto, L.T., Saeger, S., 2008, *ApJ*, 685, 1237-1246
- Fogtmann-Schulz, A., Hinrup, B., Van Eylen, V., et al. 2014, *ApJ*, 781, 67
- Fortney, J.J., Mordasini, C., Nettelmann, N., et al 2013, *ApJ*, 775, 80
- Fortney, Jonathan J., Robinson, Tyler D., Domagal-Goldman, S., et al. 2016, arXiv:1602.06305
- Hannay, N. 2012, *Treatise on Solid State Chemistry: Volume 6A* (Springer Science & Business Media)
- Howard, A. W., Sanchis-Ojeda, R., Marcy, G. W., et al. 2013, *Nature*, 503
- Howe, A. R., Burrows, A. S., 2012, *ApJ*, 756, 176
- Hui, L., Seager, S., 2002, *ApJ*, 572, 540-555.
- Hu, R., Seager, S., Bains, W., 2012, *ApJ*, 761, 166
- Hu, R., Seager, S., Bains, W., 2013, *ApJ*, 769, 6
- Hu, R., Saeger, S., 2014, *ApJ*, 784, 63
- Jacobson, N. S., Copland, E. H., Mehrotra, G. M., et al. 2002, *Electrochem. Soc. Proc.*, 226-232
- Léger, A., Grasset, O., Fegley, B., et al. 2011, *Icarus*, 213, 1

- Madhusudhan, N. 2012, *ApJ*, 758, 36
- Martins, J. H. C., Figueira, P., Santos, N. C., Lovis, C. 2013, *MNRAS* 436, 1215-1224
- Miguel, Y., Kaltenegger, L., Fegley, B., Schaefer, L. 2011, *ApJL*, 742, L19
- Miller-Ricci Kempton, E., Zahnle, K., Fortney, J. J., 2012, *ApJ*, 745, 3
- Miller, M., Armatys, K. 2013, *The Open Thermodynamics Journal*, 7, 2
- Nakayama, A., Niimi, K., Ono, Y., Taketsugu, T. 2012, *J. Chem. Phys.* 136, 54506
- Rouan, D., Deeg, H. J., Demangeon, O., et al. 2011, *ApJL*, 741, L30
- Schaefer, L., Lodders, K., Fegley, B., 2012, *ApJ*, 755, 41
- Seager, S., Sasselov, D.D., 1998, *ApJ*, 502, L157-L161.
- Seager, S., Sasselov, D.D., Theoretical Transmission Spectra during Extrasolar Giant Planet Transits, 2000, *ApJ*, 537, 916-921.
- Shukla, A. K., Banik, S., Dhaka, R. S., et al. 2004, *Review of Scientific Instruments*, 75, 4467
- Smith, B. C. 2011, *Fundamentals of Fourier Transform Infrared Spectroscopy* (2nd Ed., CRC Press)
- Winn, J. N., Matthews, J. M., Dawson, R. I., et al. 2011, *ApJL*, 737, L18

APPENDICES

Appendix A - Analysis of Spectral Data Code

```
clc
set(0,'DefaultFigureWindowStyle','docked')
warning('off','MATLAB:polyfit:RepeatedPointsOrRescale')

cd('C:\Users\davescrew\Desktop\Spectra'); %Automatically starter
Y = 1;
y = 1;
N = 0;
yup = 0;
warm = 1;
cold = 0;
MMMtrue = 0;
promptgrowthtime = 0;

%%USER INPUT
disp('IMPORTANT INFORMATION')
disp('All growth files should be save as Growth_"number" and be an N-by-2 matrix.')
disp('All background files should be saved as Background_"description" and be an N-by-2 matrix')
disp('All peak ranges files should be saved as Growth"number"_PeakRanges and be an n-by-2 matrix.')
disp('All growth times should be save as Growth_Times and be an m-by-1 matrix.')
disp('All files should be comma delimited files.')
disp('N: the total number of data points collected for one acquisition.')
disp('n: the total number of unique spectral features to be examined.')
disp('m: the total number of unique spectra acquired during growth.')
disp('Press any key to continue.')
pause
clc

userfile = input('Folder containing the Growth Files? \n','s');
cd(userfile)

promptauto = input('Would you like to auto fit all spectra? Y or N \n(This is meant for a quick view. It will not save the data or figures.)\n');

promptbackground = input('Which Background would you like to use? (Format: Background_"text") \nEnter text: ','s');

growthnumber = input('The Number of Spectral Growths? \n');
m = int2str(growthnumber);
```

```

promptversion = input('Would you like to view a specific region(s) over all the growths?
Y or N \n');

if promptversion == 1

    promptgrowthtime = input('Do you have a growth times file? Y or N \n(This assumes
you have your spectral ranges as well)\n');
    if promptgrowthtime == 1
        GrowthParameters = csvread('Growth_Times.csv');
        promptgrowthmatrix = GrowthParameters(:,1);
        NumberofSpectralFeatures = nnz(GrowthParameters(:,2));
        specificrange = GrowthParameters(1:NumberofSpectralFeatures,2:3);
    else
        specificrange = input('Which region(s)? \n(Format: [L1 U1; L2 U2; ...]) \n');
    end

    RegionAmount = size(specificrange,1);
    MMM = zeros(growthnumber,4,RegionAmount);

end

filenameB = strcat('Background_',promptbackground,'.CSV');
B = csvread(filenameB);

clc
for nn = 1:growthnumber
    nns = int2str(nn);

    if promptversion == 1
        growthrange = specificrange;
    else
        growthrangestring = strcat('Growth',nns,'_PeakRanges.csv');
        growthrange = csvread(growthrangestring);
    end

    WN = growthrange;
    WNR = size(WN,1);

    filenameG = strcat('Growth_',nns,'.CSV');
    G = csvread(filenameG);

    for n = 1:WNR

```

```

z1 = WN(n,1);
sz1 = int2str(z1);
z2 = WN(n,2);
sz2 = int2str(z2);
LowerBoundCheck = 1;
UpperBoundCheck = 1;
RangeIndexL = 0;

while LowerBoundCheck > 0
    RangeIndexL = RangeIndexL + 1;
    LowerBoundCheck = z1 - B(RangeIndexL,1);
end

RangeIndexU = RangeIndexL;
while UpperBoundCheck > 0
    RangeIndexU = RangeIndexU + 1;
    UpperBoundCheck = z2 - B(RangeIndexU,1);
end

G1 = G(RangeIndexL:RangeIndexU,2);
B1 = B(RangeIndexL:RangeIndexU,2);

SpectraMath = log(B1./G1);
X = B(RangeIndexL:RangeIndexU,1);

figure
subplot(2,1,1)
plot(X,SpectraMath)
titlerawmath = strcat('Growth ',nns,' Spectral Math');
title(titlerawmath)
xlabel('Wavenumber \fontsize{9} (cm^{-1})')
ylabel('\fontsize{15} \alpha')

subplot(2,1,2)
plot(X,G1,X,B1)
titleraw = strcat('Growth ',nns,' Raw');
title(titleraw)
xlabel('Wavenumber \fontsize{9} (cm^{-1})')
ylabel('Intensity')

hold on

prompt = input('Are there Spectral Features? Y or N \n');

if prompt == 1
    Peak1 = 0;

```

```

peakcheck = 1;
peakvalue = max(SpectraMath);
while peakcheck ~= 0
    Peak_i = Peak_i + 1;
    peakcheck = peakvalue - SpectraMath(Peak_i);
end
peakvaluex = X(Peak_i);
opp = polyfit(X(Peak_i-3:Peak_i+3),SpectraMath(Peak_i-3:Peak_i+3),2);
oppvaluex = roots(opp);
end

prompt3 = 0;
while prompt == 1

if prompt3 == 1
    prompt2 = input('Range? (Format: [Lower_Bound Upper_Bound]) \n');
    Lower = prompt2(1);
    Upper = prompt2(2);
else
    Lower = oppvaluex(2);
    Upper = oppvaluex(1);
end

i = 0;
ii = 0;
LowerCheck = 1;
UpperCheck = 1;

while LowerCheck > 0
    i = i+1;
    LowerCheck = Lower - X(i);
end
if i > 1
i = i-1;
end

while UpperCheck > 0
    ii = ii+1;
    if ii <= size(X,1)
        UpperCheck = Upper - X(ii);
    else
        UpperCheck = -1;
        ii = ii - 1;
    end
end
end

```



```

title(titleraw)
xlabel('Wavenumber \fontsize{9}(cm^{-1})')
ylabel('Intensity')

subplot(2,2,4)
plot(X,SMFitted,'--r',X,SpectraMath)
title('Polynomial Fit to Original')
xlabel('Wavenumber \fontsize{9}(cm^{-1})')
ylabel('\fontsize{15} \alpha')

if promptauto == 1
    prompt6 = 0;
else
    prompt6 = input('Would you like a different ordered fit? Y or N \n');
end

if prompt6 == 1
    prompt4 = 1;
else
    prompt4 = 0;
    yup = 1;
end

end

yarea2 = SpectraMath(i:ii);
xarea = X(i:ii);
yarea = SMCalc(i:ii);

PeakValueFitted = max(yarea);
PeakValueNotFitted = max(yarea2);
AreaNotFitted = trapz(xarea,yarea2);
Area = trapz(xarea,yarea);

PeakWavenumberCheck = 1;
iii = i - 1;
while PeakWavenumberCheck ~= 0
    iii = iii + 1;
    PeakWavenumberCheck = PeakValueNotFitted - SpectraMath(iii);
end

PeakWavenumberCheck2 = 1;
iiii = i - 1;
while PeakWavenumberCheck2 ~= 0
    iiii = iiii + 1;
    PeakWavenumberCheck2 = PeakValueFitted - SMCalc(iiii);
end

```



```

end

PeakWavenumber = X(iiii);
PeakWavenumberNotFitted = X(iii);

txtstring2 = sprintf('\n Area: %0.5g \n (%0.5g , %0.3g) \n %0.5g to %0.5g
',AreaNotFitted,PeakWavenumberNotFitted,PeakValueNotFitted,X(i),X(ii));
txtstring = sprintf('\n Area: %0.5g \n (%0.5g , %0.3g) \n %0.5g to
%0.5g',Area,PeakWavenumber,PeakValueFitted,X(i),X(ii));
txtstring3 = sprintf('\n \n %0.2g Order Fit',prompt5);
textxlocalcheck = (max(X)-PeakWavenumber)/(max(X)-min(X));
if textxlocalcheck <= 0.4
    xlocale = X(2);
else
    xlocale = X(iiii+4);
end

if yup == 1
    subplot(2,2,1)
    text(xlocale,0.9*(max(SpectraMath(i:ii))-
min(SpectraMath(i:ii)))+min(SpectraMath(i:ii)),txtstring2)
    subplot(2,2,2)
    text(xlocale,0.9*(max(SMCalc(i:ii))-
min(SMCalc(i:ii)))+min(SMCalc(i:ii)),txtstring)
    subplot(2,2,4)
    text(xlocale,0.9*(max(SpectraMath(i:ii))-
min(SpectraMath(i:ii)))+min(SpectraMath(i:ii)),txtstring3)
else
    subplot(2,1,1)
    text(xlocale,0.9*(max(SpectraMath(i:ii))-
min(SpectraMath(i:ii)))+min(SpectraMath(i:ii)),txtstring2)
end

if promptauto == 1
    prompt3 = 0;
else
    prompt3 = input('Would you like to try a different Spectral Feature Range? Y or N
\n');
end

if prompt3 == 0
    MMM(nn,2,n) = Area;
    MMM(nn,3,n) = PeakValueFitted;
    MMM(nn,4,n) = PeakWavenumber;
    MMMtrue = 1;
    prompt = 0;

```

```

end
end

if yup == 0
    Xlength = size(X);
    SMCalc = zeros(Xlength(1));
end

if promptauto == 1
    prompt7 = 0;
else
    prompt7 = input('Would you like to save Data and Graphs? Y or N \n');
end

if prompt7 == 1
    Data = horzcat(X,SpectraMath,SMCalc);
    GrowthDat = strcat('Growth',nns,'_',promptbackground,'_Math_',sz1,'_',sz2,'.dat');
    GrowthGraph =
    strcat('Growth',nns,'_',promptbackground,'Graph_Math_',sz1,'_',sz2,'.jpg');
    saveas(gcf,GrowthGraph);
    csvwrite(GrowthDat,Data);
end

hold off
yup = 0;

if promptgrowthtime == 1
    MMM(nn,1,n) = promptgrowthmatrix(nn);
else
    MMM(nn,1,n) = nn;
end

clc
end
end

if promptversion == 1 && MMMtrue == 1
    for nntp = 1:RegionAmount

        RangeTimePlot1 = specificrange(nntp,1);
        RangeTimePlot2 = specificrange(nntp,2);
        timepoly1 =
        polyfit(MMM(1:growthnumber,1,nntp),MMM(1:growthnumber,2,nntp),1);
        timepoly2 =
        polyfit(MMM(1:growthnumber,1,nntp),MMM(1:growthnumber,3,nntp),1);
    end
end

```

```

timepoly3 =
polyfit(MMM(1:growthnumber,1,nntp),MMM(1:growthnumber,4,nntp),1);
polyplotrange = MMM(1:growthnumber,1,nntp);
polyploty1 = polyval(timepoly1,polyplotrange);
polyploty2 = polyval(timepoly2,polyplotrange);
polyploty3 = polyval(timepoly3,polyplotrange);

figure
subplot(3,1,1)

plot(MMM(1:growthnumber,1,nntp),MMM(1:growthnumber,2,nntp),'o',polyplotrange,polyploty1,'--r')
timetitleplot = sprintf('Progression of the Area: %0.5g to %0.05g',RangeTimePlot1,RangeTimePlot2);
title(timetitleplot)
polytextheight1 = 0.9*(max(MMM(1:growthnumber,2,nntp))-min(MMM(1:growthnumber,2,nntp)))+min(MMM(1:growthnumber,2,nntp));
txt1 = sprintf('y(x) = %0.3g (x) + %0.3g',timepoly1(1),timepoly1(2)) ;
text(polyplotrange(1),polytextheight1,txt1)
ylabel('Intensity')

subplot(3,1,2)

plot(MMM(1:growthnumber,1,nntp),MMM(1:growthnumber,3,nntp),'o',polyplotrange,polyploty2,'--r')
timetitleplot2 = sprintf('Progression of the Peak Value: %0.5g to %0.05g',RangeTimePlot1,RangeTimePlot2);
title(timetitleplot2)
polytextheight2 = 0.9*(max(MMM(1:growthnumber,3,nntp))-min(MMM(1:growthnumber,3,nntp)))+min(MMM(1:growthnumber,3,nntp));
txt2 = sprintf('y(x) = %0.3g (x) + %0.3g',timepoly2(1),timepoly2(2)) ;
text(polyplotrange(1),polytextheight2,txt2)
ylabel('Intensity')
subplot(3,1,3)

plot(MMM(1:growthnumber,1,nntp),MMM(1:growthnumber,4,nntp),'o')%,polyplotrange,polyploty3,'--r')
timetitleplot3 = sprintf('Progression of the Peak Wavenumber: %0.5g to %0.05g',RangeTimePlot1,RangeTimePlot2);
title(timetitleplot3)
% polytextheight3 = 0.9*(max(MMM(1:growthnumber,4,nntp))-min(MMM(1:growthnumber,4,nntp)))+min(MMM(1:growthnumber,4,nntp));
% txt3 = sprintf('y(x) = %0.3g (x) + %0.3g',timepoly3(1),timepoly3(2)) ;
% text(polyplotrange(1),polytextheight3,txt3)
xlabel('Growth Time \fontsize{9} (seconds)')
ylabel('Wavenumber \fontsize{9} (cm^{-1})')

```

```

        promptsavetimeprogression = input('Would you like to save the Time Progression
data and graphs? Y or N \n');
        if promptsavetimeprogression == 1
            txt4 =
sprintf('Time_Progression_%.3g_to_%.3g.dat',RangeTimePlot1,RangeTimePlot2);
            txt5 =
sprintf('Time_Progression_%.3g_to_%.3g.jpg',RangeTimePlot1,RangeTimePlot2);
            csvwrite(txt4,MMM(:,nntp))
            saveas(gcf,txt5);
        end
        clc
        end
    elseif promptversion == 1 && MMMtrue == 0
        disp('There were no spectral features in the specified Range(s).')
    end

prompt99 = input('Would you like to save any of the figures to .pdf file? Y or N\n');
if prompt99 == 1
    prompt999 = input('Which figures would you like to save? (Format: [1 2 3 ... n]) \n');
    NumberofSaved = size(prompt999,2);

    for w = 1:NumberofSaved
        figurenumber = prompt999(w);
        figure(figurenumber)
        figurenumberstring = int2str(figurenumber);
        fns = strcat('figure',figurenumberstring);
        saveas(gcf,fns,'pdf')
    end

end

promptpeakdetermine = input('Would you like to attempt to find peak(s) in the database?
Y or N \n');
if promptpeakdetermine == 1
    cd('C:\Users\davescrew\Desktop\Spectra');
    [xxx,word,row] = xlsread('Database_updated.xlsx','C3:D300');
    xxxvalue = MMM(end,4,:); %input('Which Peak(s) would you like to find?
(Format:[Peak1; Peak2; etc..]) \n');
    xxxvaluesize = size(xxxvalue);
    tolerance = 5; %input('What tolerance would you like to find your Peak? \n');
    clc

    for nn = 1:xxxvaluesize(1,3)
        BB = find(xxx < xxxvalue(nn)+tolerance & xxx > xxxvalue(nn)-tolerance);

```

```

BBamount = size(BB,1);
if BBamount == 0
disp('No molecules matched your peak locations with 5 wavenumbers');
else
    for n = 1:BBamount

        txttxt2 = strcat(word(BB(n)), ' is the Chemical Formula');
        txttxt = sprintf('The closest peak value(s): %0.7g for the %0.7g
entry.',xxx(BB(n)),xxxvalue(nn));

        disp(txttxt)
        disp(txttxt2)
    end
end
end
disp('Peaks are found within 5 wavenumbers of values entered.')
end

warning('on','MATLAB:polyfit:RepeatedPointsOrRescale')

h = msgbox({'Thank you for using Gemar Softwares.', 'Where we be gettin dat
data...'});

```

Appendix B - Emissivity Correction Code

```
clear all
clc
warning('off','MATLAB:polyfit:RepeatedPointsOrRescale')

ZZ = 1; %Step Size in C
ZMin = 0;%Min Temp in C
ZMax = 3000; %Max Temp in C
Z = (ZMax - ZMin)/ZZ + 1; %Number of Points
ZZZ = ceil(Z);
M = 1:Z;

Eused = .18; %Emissivity used
Y = [.14 .19 .26 .30];
XC = [727 1093 1982 2930];
X = XC + 273;
Poly = polyfit(X,Y,2);

TempWantC = ZMax - (M-1)*ZZ;
TempWant = TempWantC + 273;

Evalureal = polyval(Poly,TempWant);

TempMeasure = TempWant .* (Evalureal/Eused).^25;
TempMeasureC = TempMeasure - 273;

TempMeasureCL = TempMeasureC.';
TempWantCL = TempWantC.';

MC = cat(2,TempWantCL,TempMeasureCL);
MR = cat(1,TempWantC,TempMeasureC);

Poly2 = polyfit(TempMeasureC,TempWantC,3);
% for n = 1:5
% Poly3 = polyfit(TempMeasureC,TempWantC,n);
% figure
% plot(MC(:,2),MC(:,1),'o',MC(:,2),polyval(Poly3,MC(:,2)),'--r')
% txt = sprintf('Polynomial fit of Order %0.5g',n);
% title(txt)
% end
TempMeasured = 1;
while TempMeasured ~= 0

TempMeasured = input('What Temperature are you measuring?\n');
Temp = polyval(Poly2, TempMeasured);
```

```
txt = sprintf('Temperature of Crucible: %0.5g C',Temp);  
disp(txt)  
  
end
```